

THE MECHANICAL RESPONSE OF AN AL ALLOY  
REINFORCED WITH SIC

THE MECHANICAL RESPONSE OF AN Al ALLOY  
REINFORCED WITH SIC

By

GILLES BEAULIEU, B.Sc.A.

A Thesis

Submitted to the School of Graduate Studies  
in Partial Fulfilment of the Requirements  
for the Degree  
Master of Engineering

McMaster University

(c) Copyright by Gilles Beaulieu, April 1991

**MASTER OF ENGINEERING (1991)**

**MCMASTER UNIVERSITY**

**(Materials Science and Engineering)**

**Hamilton, Ontario**

**TITLE: The Mechanical Response of an Al Alloy**

**Reinforced with SiC**

**AUTHOR: Gilles Beaulieu, B.Sc.A. (Université Laval)**

**SUPERVISOR: Professor J.D.Embury**

**NUMBER OF PAGES: xii, 118**

## ABSTRACT

This study investigated the role of SiC particles in the mechanical behaviour of a metal matrix composite (Al-SiC). Measurements of the development and magnitude of internal stresses were performed from Bauschinger experiments in the aluminum matrix A-356 reinforced with the SiC particles. The behaviour of the Al matrix itself was also analyzed.

The level of internal stresses in the particulate reinforced composite was found to saturate after 0.9% plastic strain and after 1.3% in the unreinforced matrix. The initial development of the unrelaxed internal stresses was analyzed using both microscopic and macroscopic models of the load bearing role of the SiC particles.

The SiC particles were found to have little influence on the plastic flow of the composite beyond the initial plastic deformation as the size and distribution of the SiC is very non uniform. The effect of the SiC phase was compared to continuous fibres embedded in a metallic matrix. A model system of pure copper reinforced with continuous tungsten fibres was used for this purpose.

The effect of the internal stresses on the dimensional stability of the particulate reinforced and the unreinforced matrix was also investigated. The generation of dislocations arising from the thermal cycling of those materials was also analyzed by reference to the increase in flow stress observed after thermal cycling and from a model based on dislocations production due to the difference in coefficient of thermal expansion of the phases.

## ACKNOWLEDGMENT

The author would like to express his gratitude to professor J.D.Embury for his guidance and advice throughout the course of this work

Thanks are also due to the "Fonds pour la formation des chercheurs et l'aide à la recherche" (Fonds FCAR) for financial support, and to Alcan International Ltd., KRDC, for providing the alloy and particulate composite materials used in this study. In addition, thanks go to Warren Poole for the preparation of the continuous fibre composite material.

Finally, the author would like to thanks the mechanical metallurgy group for the discussions and help. And for the english lessons, spanish lessons, chinese lessons, tennis lessons, squash lessons, French cooking lessons, ... etc..

# TABLE OF CONTENTS

	Page
ABSTRACT.....	iii
ACKNOWLEDGMENTS.....	v
TABLE OF CONTENTS.....	vi
LIST OF FIGURES.....	viii
LIST OF TABLES.....	xii
CHAPTER 1: INTRODUCTION.....	1
CHAPTER 2: LITERATURE REVIEW.....	5
2.1 Internal Stresses in Composite Materials.....	5
2.2 Measurement Methods.....	15
2.3 Dimensional Instability.....	19
2.4 Thermal Cycling.....	20
CHAPTER 3: EXPERIMENTAL PROCEDURES.....	26
3.1 Materials.....	26
3.1.1 Aluminum Based Materials.....	26
3.1.2 Copper-Tungsten Composite.....	30
3.2 Mechanical Testing.....	33
3.2.1 Introduction.....	33
3.2.2 Bauschinger Experiment.....	33

3.2.3	Stress-Strain Measurement.....	41
3.2.4	Dimensional Instability	
	Experiment.....	44
<b>CHAPTER 4:</b>	<b>RESULTS.....</b>	<b>49</b>
4.1	Introduction.....	49
4.2	Mechanical Response of the Unreinforced and Particulate Composite Materials.....	50
4.3	Dimensional Instability.....	73
4.4	Mechanical Properties of the Copper Tungsten Composite.....	76
<b>CHAPTER 5:</b>	<b>DISCUSSION.....</b>	<b>83</b>
5.1	Model System Based on Copper with Continuous Tungsten Fibres.....	83
5.2	Monotonic Loading of the SiC <sub>p</sub> Composite and Unreinforced Materials.....	88
5.3	Reverse Loading of the SiC <sub>p</sub> Composite and Unreinforced Materials.....	91
5.4	Thermally Cycled Specimens.....	104
5.5	Dimensional Instability.....	109
<b>CONCLUSIONS.....</b>		<b>114</b>
<b>REFERENCES.....</b>		<b>116</b>

## LIST OF FIGURES

	Page
Figure 2.1 Continuous aligned fibre composite.....	8
Figure 2.2 Stress strain curve of continuous aligned fibre reinforced metal matrix composite.....	8
Figure 2.3 Stress strain curve with a) an ideal elastic plastic transition and b) a transition which occurs over a wide range of strain.....	11
Figure 2.4 Microstructure of a single phase polycrystal prior plastic deformation.....	12
Figure 2.5 Accumulation of dislocations and build up of internal stresses at the grain boundary of a single phase polycrystal during deformation.....	12
Figure 2.6a Microstructure of a single phase polycrystal containing a second phase particle, the size of the matrix grain, prior plastic deformation.....	14
Figure 2.6b Submicron size second phase particle stressed by dislocations.....	14
Figure 2.7 Schematic representation of an hysteresis loop and the Bauschinger effect.....	17
Figure 2.8 Schematic representation of the permanent softening.....	17
Figure 2.9 Diagram of a particle and several punched dislocations.....	24
Figure 3.1 Micrograph of the composite material Al-SiC.....	29

Figure 3.2	Aluminum-Silicon phase diagram.....	31
Figure 3.3	Graphite mould used in the making of Cu/W specimens.....	32
Figure 3.4	Cross-section of a Cu/W specimen.....	34
Figure 3.5	Partial drawing of the Bauschinger rig.....	36
Figure 3.6	Set-up of the Bauschinger rig on the Instron tension compression tester.....	37
Figure 3.7	Specifications for the Bauschinger experiments specimens.....	39
Figure 3.8	Alignment rig used to set-up the specimens in the grips.....	40
Figure 3.9	Close-up at the Bauschinger rig showing a specimen in the grips and the extensometer used.....	42
Figure 3.10	Load cell calibration curve.....	43
Figure 3.11	Extensometer calibration curve at +25°C.....	45
Figure 3.12	Extensometer calibration curve at -50°C.....	46
Figure 3.13	Specimen used for the dimensional instability experiments and the flat ended cylinders used for the compression.....	48
Figure 4.1	Hysteresis loops for the unreinforced material, R.T.. Tension first testing only...	58
Figure 4.2	Hysteresis loops for the unreinforced Material, -50°C. Tension first testing only.....	59
Figure 4.3	Hysteresis loops for the particulate composite material, R.T.. Tension first testing only.....	60
Figure 4.4	Hysteresis loops for the particulate composite material, -50°C. Tension first testing only.....	61
Figure 4.5	Typical Bauschinger experiment result for the unreinforced material showing no measurable permanent softening.....	62

Figure 4.6	Typical Bauschinger experiment result for the particulate composite material showing no measurable permanent softening.....	63
Figure 4.7	Backstress measurement results for the particulate composite material, $10^4$ yield offset.....	64
Figure 4.8	Backstress measurement results for the particulate composite material, $10^3$ yield offset.....	65
Figure 4.9	Backstress measurement results for the unreinforced material, $10^4$ yield offset.....	66
Figure 4.10	Backstress measurement results for the unreinforced material, $10^3$ yield offset.....	67
Figure 4.11	Hysteresis loop for the particulate composite for two specimens tested in compression-tension and two specimens tested in tension compression.....	70
Figure 4.12	Stress strain curves of thermally cycled particulate composite material with non thermally cycled specimens.....	71
Figure 4.13	Stress strain curves of thermally cycled unreinforced material with non thermally cycled specimens.....	72
Figure 4.14	Dimensional instability results for the particulate composite material.....	74
Figure 4.15	Dimensional instability results for the unreinforced material.....	75
Figure 4.16	Stress strain curve of the Cu/W composite specimen #1.....	78
Figure 4.17	Stress strain curve of the Cu/W composite specimen #2.....	79
Figure 4.18	Stress strain curve of the Cu/W composite specimen #4.....	80

Figure 4.19	Stress strain curve of the Cu/W composite specimen #6.....	81
Figure 5.1	Rate of increase of the unrelaxed backstress for different volume fraction of SiC calculated using a microscopic and a macroscopic model.....	99

## LIST OF TABLES

	Page
Table 2.1	Linear coefficient of thermal expansion (CTE) of some metal matrices and reinforcing phases..... 22
Table 3.1	Alloying elements of A-356..... 28
Table 3.2	Extensometer calibrations results..... 28
Table 4.1	Material and testing conditions of each specimen used for the Bauschinger experiments..... 51
Table 4.2	Mechanical response of each specimen used in the Bauschinger experiments..... 53
Table 4.3	Mechanical response averaged per testing conditions and material..... 55
Table 4.4	Hardness results obtained after T61 heat treatment..... 56
Table 4.5	Results from the copper tungsten composite tests..... 82
Table 5.1	Calculated elastic modulus and work hardening rate of the copper matrix in copper tungsten composites..... 85
Table 5.2	Dislocation density results ( $\Delta\rho$ ) and theoretical ( $\rho_r$ ) in the thermally cycled specimens..... 107

# CHAPTER 1

## INTRODUCTION

The mechanical response of metal matrix composites (MMCs) reinforced with continuous fibres has been the subject of extensive research (M.R.Piggott,1980, H.Lilholt,1977, O.B.Pederson,1990, A.Kelly,1964, M.Taya,1981). The recent years however have seen the introduction of particulate reinforced MMCs, in part due to the availability of low cost reinforcements and new, economical, fabrication techniques. The mechanical behaviour of these particulate reinforced materials can differ in many respects from continuously reinforced composites.

In particulate reinforced composites the heterogeneous distribution of the reinforcing phase and the shape and size of those particles are factors which can influence:

a) the elastic modulus, yield strength and the work hardening of the composite through the complex process of load transfer between the phases.

b) the development of internal elastic stresses due to the difference in both the mechanical properties and the

coefficients of thermal expansion between the reinforcing phases and the matrix.

c) the development of local stresses and stress states which can initiate damage and fracture of the reinforcing phase and ultimately of the composite.

However the scope of the present investigation has been restricted to concentrate on the low strain regime in an attempt to determine the local stresses carried out by the reinforcements and the role of these stresses, both in relation to the load bearing characteristics of the composite and the process of damage initiation, in particulate composites. To provide a context for the behaviour of these materials the relation between the mechanical response of continuously reinforced MMCs and particulate MMCs has also been examined.

The materials used in the present work were a model system made of pure copper reinforced with continuous longitudinal fibres of tungsten, a particulate composite made by Alcan Ltd. consisting of an aluminum matrix A-356 reinforced with 20% volume fraction of SiC and finally the unreinforced matrix A-356.

In order to investigate the low strain regime, three distinct sets of experiments were performed:

1. Tensile loading experiments and Bauschinger tests. These were used to analyze the monotonic loading behaviour and the behaviour during strain reversals. The change in strain path of deformation, i.e. the strain reversal in Bauschinger tests, allows an evaluation of the internal elastic stresses developed in the materials during the initial tensile strain increment.

2. Dimensional instability experiments. Plastically induced internal elastic stresses, when allowed to relax, cause a change in the dimensions of the specimens. The internal stresses can therefore be evaluated using the magnitude of this dimensional instability. Both the particulate reinforced composite and its unreinforced matrix were tested to determine the extent of dimensional instability.

3. Tensile loading of previously thermally cycled specimens. The effect of the difference in the coefficients of thermal expansion between the reinforcing phase and its matrix on the tensile loading behaviour (of the particulate composite and its matrix) were investigated in order to determine the influence of thermally induced stresses on the mechanical response.

The tensile and Bauschinger testing were limited to a

maximum of 2% plastic strain. In order to study the influence of the deformation temperature on the development and relaxation of the internal stresses, the Bauschinger experiments were performed at +25°C and -50°C.

## **CHAPTER 2**

### **LITERATURE REVIEW**

This chapter has been divided in four sections covering the different aspects that are the subject of this work. The first section will introduce the concept of development of internal stresses, with particular emphasis on composite materials, as these materials are plastically strained. The different measurement techniques will then be described and the influence of the residual stresses in materials on their dimensional instability will also be discussed. Finally this chapter will end with a review of different methods of analyzing the effect of thermal cycling on the mechanical behaviour of particulate reinforced composites.

#### **2.1 Internal Stresses in Composite Materials:**

The residual internal stresses in a material or structure arise from the presence of a heterogeneous elastic strain state in the microstructure of these. Such internally stressed materials have their basic mechanical properties modified by these internal stresses and as a result their

expected behaviour in their environment can be altered. The yield strength as well as the ductility of a material for example can be greatly changed (J.Friedel,1959).

Diverse factors can serve as the origin of the presence of residual strains in the microstructure of a material and they can be classified into two categories. The first one is the effect of non uniform external forces on a material which cause it to be strained heterogeneously. A good example of this occurs when a beam is bent until it becomes permanently deformed; one of the surfaces remains under tension and the other in compression after the removal of the load. The non-uniform heating (e.g. in welding) or chemical reaction (e.g. surface carburizing of steel) along with non-uniform applied stresses are different examples of this category.

The second category of internal stresses is the subject of this work and arises from the presence of inhomogeneities such as a reinforcing phase in the microstructure of the material. Internal stresses in composite materials can first develop during the plastic deformation of the material because of the heterogeneous deformation of the microstructure and second from the different coefficient of thermal expansion between the phases. In both cases elastic strains are developed non uniformly in the material and thus

a residual stress (or strain) state remains.

The understanding of the development of the internal stresses during the deformation of composite materials can be conveniently shown by dividing the deformation curve (stress strain curve) into three distinct parts; the elastic loading, the transition from elastic to plastic deformation and finally the fully plastic regime. The reinforcing phases in this work (tungsten and silicon carbide) deform only elastically (unless they reach their fracture strength) during the deformation of the composites.

During the elastic loading of a simple composite material containing continuous reinforcing fibres (of a greater stiffness than the matrix) aligned in the loading axis of the material (see figure 2.1), the strain seen by the different phases is the same but the stress they are subjected to is not. This is illustrated in figure 2.2 at a level of deformation "a" of the composite. The stress state in the material in this early stage of deformation can be described, if the fibres are uniformly distributed in the cross-section, using the well proven rule of averages for the stress  $\sigma$  and rule of mixtures for the modulus  $E$  (M.R.Piggott, 1980, A.Kelly and N.H.MacMillan, 1986)

$$\sigma = V_f \sigma_f + V_m \sigma_m \quad (2.1)$$

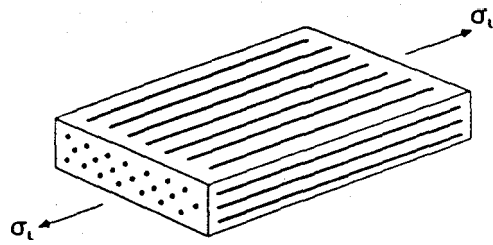


Figure 2.1 Continuous aligned fibre composite.

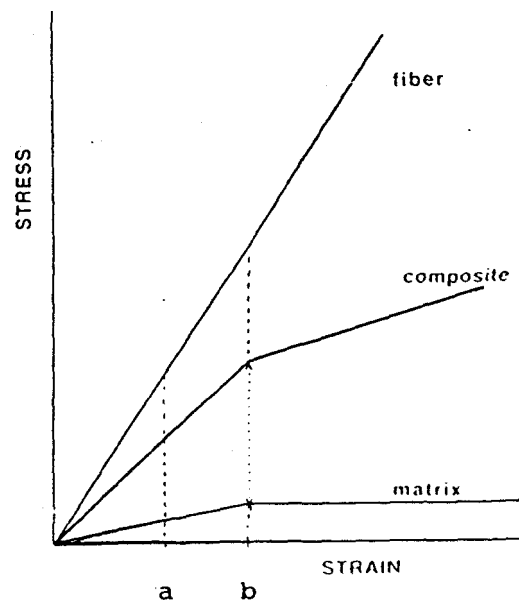


Figure 2.2 Stress strain curve of continuous aligned fibre reinforced metal matrix composite.

where the subscript f denotes fibre and m matrix and  $\sigma$  the average stress carried by the corresponding phase, and

$$E = V_f E_f + V_m E_m \quad (2.2)$$

A particulate composite presents a more complex situation since both the stress and strain seen by the reinforcing phases are different from those of the matrix. The stress a single particle and its surrounding matrix is subjected to is difficult to evaluate if the shape of the particle is intricate. The distribution of internal elastic stresses in particulate composites is therefore very complex and cannot be readily modeled as for composites reinforced by long fibres.

These complex internal elastic stress states in particulate composites affect the beginning of the plastic deformation of the matrix and therefore the composite's flow curve. The relatively simple stress states in continuously reinforced composites does allow the transition from the elastic to plastic deformation of the composite to be rapid. The matrix is essentially everywhere under the same stress state and therefore begins to flow throughout the composite at approximately the same level of strain "b" in figure 2.2. The matrix in particulate composites however begins to deform plastically in regions where the level of internal elastic

stress is high before other regions where, due to the inhomogeneity of the microstructure, the matrix is under less stress. The transition to plastic deformation is thus a process scaled over a wide range of strain during which different regions of the matrix become sequentially into the plastic deformation regime (figure 2.3). The reinforcing phase in this process can even become, in some locations, subjected to stresses high enough to fracture them.

When the matrix eventually reaches the fully plastic regime, some of the regions of the matrix might have plastically deformed extensively. The heterogeneous plastic deformation of the matrix in particulate composites implies that residual stresses will be present in the composite after unloading. By analogy with the plastic deformation of a polycrystal, it is possible to appreciate that residual internal stresses can develop during the inhomogeneous plastic deformation of a microstructure even when no reinforcing phases are present. Figure 2.4 illustrates the microstructure of a single phase metal having grains of different orientation relative to the loading axis of the material. A dislocation moving across one of the grains is not likely to be able to cross into a neighbouring grain due to the different crystallographic orientation of that second grain relative to the first. The dislocations thus pile up at the grain boundary until a stress is reached at which the second grain's

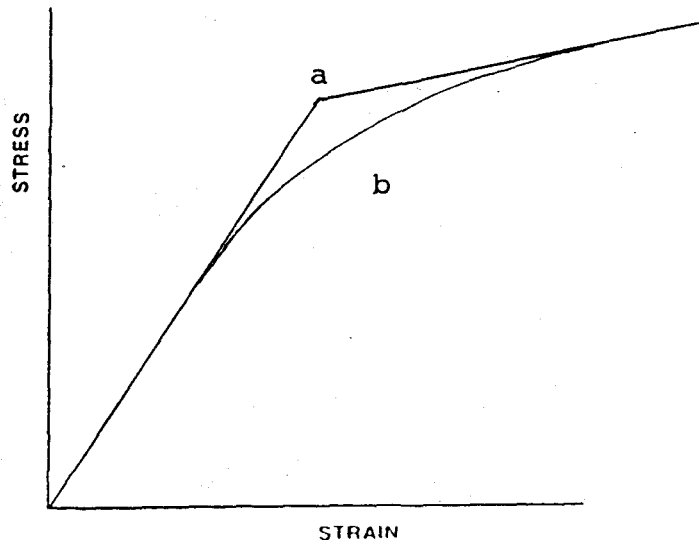


Figure 2.3 Stress strain curve with a) an ideal elastic plastic transition and b) a transition which occurs over a wide range of strain.

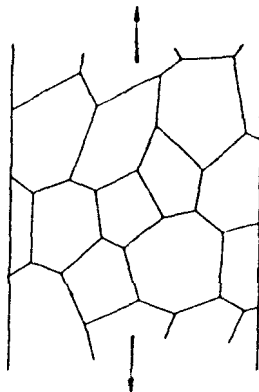


Figure 2.4 Microstructure of a single phase polycrystal prior plastic deformation.

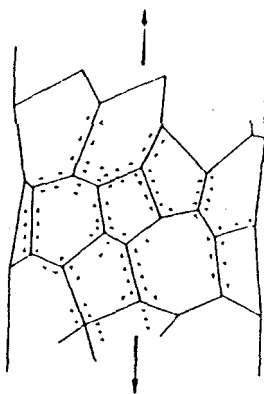


Figure 2.5 Accumulation of dislocations and build up of internal stresses at the grain boundary of a single phase polycrystal during deformation.

dislocations begin to be activated. The extent of the accumulation of dislocations varies from one grain to another and thus is a non-uniform process. The different grains therefore develop internal stresses due to this pile-up of dislocations at their grain boundary (figure 2.5). The addition of second phases like particulates provides other mechanisms to build up elastic stresses. If these particles are on the micrometer scale their effect can be viewed similarly to the case of grains of different stiffness and yield strength (figure 2.6a), and smaller particles than those can accumulate loops of dislocations around them (figure 2.6b).

It is possible to anticipate that the build up of internal elastic stresses will increase as the imposed deformation is also increased. The fracture of the reinforcing phases and other mechanisms of relaxation however can also occur as the deformation is increased and therefore the magnitude of the internal stresses can reach a saturation level after a given imposed deformation.

The flow curve of continuously reinforced composites during plastic deformation has been described in the literature for those materials. The more complex microstructure and stress state of particulate composites however makes such evaluation very difficult.

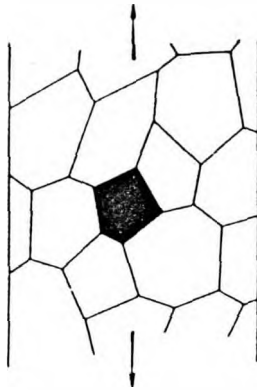


Figure 2.6a Microstructure of a single phase polycrystal containing a second phase particle, the size of the matrix grain, prior plastic deformation.



Figure 2.6b Submicron size second phase particle stressed by dislocations.

## 2.2 Measurement Methods:

The residual elastic stresses developed during plastic deformation of composites can be determined using direct measurement methods such as diffraction techniques (X-rays or neutrons) or by indirect methods such as the effect of the internal stresses on the mechanical response of the material.

The X-ray and neutron diffraction techniques have been used on Al-SiC particulate composites (H.M.Ledbetter et al., 1987, A.J.Allen et al., 1987). These methods use the change in lattice spacing in one of the two phases (either the matrix or the reinforcement) arising from the internal elastic stresses as a measurement of the residual strain. Provided that the unloading and the preparation of the material is adequately done to minimize the relaxation of the elastic stresses in the material, the methods can give valuable estimations of these stresses (D.V.Wilson and Y.A.Konnan, 1964). The evaluation of the level of internal stresses present in a material however is usually made from mechanical testings such as the Bauschinger experiment (A.H.Cottrell, 1953, R.L.Woolley, 1953, L.M.Brown and W.M.Stobbs, 1971, K.Tanaka and T.Mori, 1970).

Bauschinger (1886) observed that after deforming a material plastically in tension (or compression), the yield strength in the reverse direction (compression or tension) is

lowered. This yield lowering effect was also found to be dependent on the level of the forward plastic deformation. Figure 2.7 is a diagram that illustrates schematically this effect. The reverse flow stress  $\sigma_R$  is lower, in absolute value, than the forward flow stress  $\sigma_0$ .

The forward deformation stress  $\sigma_F$  can be described in terms of the different stress components in a material as described by Moan et al. (1979) as

$$\sigma_F = \sigma_0 + \sigma_s + \sigma_B \quad (2.3)$$

where  $\sigma_0$  is the initial yield stress of the material,  $\sigma_s$  the contribution from isotropic hardening and  $\sigma_B$  the mean directional stress in the matrix or backstress. The reverse flow strength can then be described following equation 2.3 as

$$\sigma_F = \sigma_0 + \sigma_s - \sigma_B \quad (2.4)$$

since the directional character of the backstress  $\sigma_B$  has for effect to aid the reverse flow. Therefore the larger the backstress component developed during forward deformation the less is the magnitude of the reverse flow stress.

The measurement of the backstress from a Bauschinger experiment can therefore be based on the permanent softening  $\Delta\sigma_p$  observed when the reverse flow curve is plotted in the

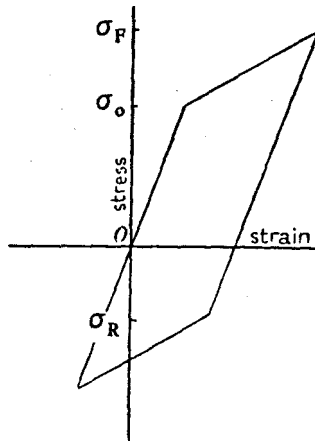


Figure 2.7 Schematic representation of an hysteresis loop and the Bauschinger effect.

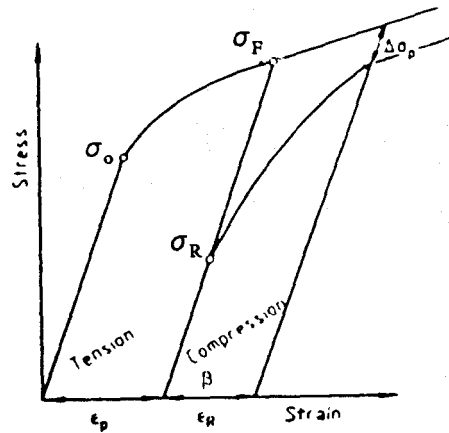


Figure 2.8 Schematic representation of the permanent softening.

forward quadrant to allow the measurement, figure 2.8. Following Atkinson et al. (1974) the evaluation of the backstress  $\sigma_B$  is then

$$\sigma_B = \Delta\sigma_P/2 \quad (2.5)$$

Such estimation of the backstress has been made since Atkinson on different dispersion hardened materials and volume fractions of particles but was found to give an underestimate in spheroidised steel (D.J.Lloyd, 1976, D.V.Wilson, 1965). This measurement method is based on the possibility of having a measurable permanent softening. Some materials require large reverse straining before obtaining parallelism with the forward strain curve while others never do become parallel.

The yield lowering effect in the Bauschinger experiment can also be used to evaluate the backstress  $\sigma_B$ . The reverse flow  $\sigma_R$  is aided by the backstress  $\sigma_B$  and its influence can thus be observed by the decrease in yield in compression. Taking equation 2.3 and subtracting 2.4 gives

$$\sigma_F - \sigma_R = 2\sigma_B \quad (2.6)$$

or

$$\sigma_B = (\sigma_F - \sigma_R) / 2 \quad (2.7)$$

where the yield stress  $\sigma_R$  in the reverse path of deformation is defined at a given level of strain offset.

The presence of residual internal elastic stresses affects mechanical properties other than the yield surface which can be used to evaluate the magnitude of these stresses. The effect of the internal stresses on the dimensional instability of a material has also been used in this study and will be described next.

### 2.3 Dimensional Instability:

A material after being deformed plastically is often observed to recover some of the plastic deformation after a given time. This recovery is small in magnitude and might represent between  $1/100^{\text{th}}$  to  $1/50^{\text{th}}$  of the total plastic deformation (C.W.Marshall and R.E.Maringer, 1977). In two phase systems the effect is larger and some investigators have found a recovery of up to  $1/5^{\text{th}}$  of the plastic strain (e.g. in normalized 4340 steel (G.W.Geil et al., 1969)). However the effect is dependent on the size and volume fraction of the second phase. Mori and Narita (1975) found in a dispersion hardened material (copper containing 0.41% volume fraction of silica of 0.12  $\mu\text{m}$  in diameter) a maximum recovery of  $1/400^{\text{th}}$  of the imposed plastic deformation.

The mechanism for this dimensional change arises due to the creep which occurs to relax the backstresses developed in the material during plastic deformation. As the material is

deformed, the dislocations accumulate against the obstacles thus creating plastic strain gradients which result in a directional elastic stress within the matrix as well as elastic stress within the obstacles. In the case of the particulate composite and unreinforced materials used in this study, the Si precipitates and the SiC particles become elastically strained. Upon removal of the load the directional character of the backstress is present in the matrix. An increase in temperature can then allow the thermally activated motion of dislocations under the influence of a backstress to overcome the barriers. As a result from this motion of dislocations in a direction to reduce the backstress, a change in the dimensions of the specimen can be observed. The magnitude of the dimensional instability can therefore reveal information on the level of backstress developed in a material during plastic deformation. The careful experiments done by Mori and Narita effectively showed a good agreement between the backstress measured after different imposed plastic deformation and the dimensional instability in the same conditions.

#### **2.4 Thermal Cycling:**

Much of the experimental (S.Yoda et al., 1979, W.G.Patterson et al., 1985) and modelling (G.Garmon, 1974, S.Yoda et al., 1978) work in the literature on thermal cycling covers the effects of such thermal treatment on the

dimensional instability and the nature of the damage produced in continuous fibre reinforced MMCs. In these fatigue studies the number of cycles performed are in the range of  $10^3$  to  $10^5$  and the temperature differential  $\Delta T$  is in the range of 200 to  $800^\circ\text{C}$  (M.Taya and R.J.Arsenault, 1989). In such fatigue tests the source of the cyclic stress relates to the extent of the thermal mismatch between the phases which arise during the thermal cycling.

In the present work the influence of small a number of thermal cycles was considered. When a composite is subjected to a thermal cycle of  $\Delta T$ , the effect of the different coefficients of thermal expansions (CTE) between the reinforcing phase and the matrix (see table 2.1) creates local elastic stresses which can be sufficient to produce a strain at the interface greater than the strain required to initiate plastic flow of the matrix. The strain mismatch  $\epsilon$  can then be defined in terms of  $\Delta T$  and  $\Delta\text{CTE}$  as

$$\epsilon = \Delta\text{CTE} \cdot \Delta T \quad (2.8)$$

and therefore with all the materials listed in table 2.1 a difference in temperature of  $200^\circ\text{C}$  creates a strain greater than  $2 \times 10^{-3}$ . The strain at the interface between the matrix and the reinforcing phase may therefore create dislocations in the thermal cycling process and indeed an increase in dislocation density in dispersion hardened materials and other

	CTE ( $\times 10^{-6}/^{\circ}\text{C}$ )
Al	24
Cu	16.5
W	4.5
SiC	4
Si	2.5

Table 2.1 Linear coefficient of thermal expansion (CTE) of some metal matrices and reinforcing phases (From M.Taya and R.J.Arsenault, 1989)

materials containing second phase particulates has been observed (K.K.Chawla and M.Metzger,1972, M.F.Ashby et al., 1969, R.J.Arsenault and R.M.Fisher,1983).

The main effect of this increase in the density of dislocations is the increase in the flow stress. Knowing the increase in flow stress  $\Delta\sigma$  after thermal cycling thus allows a crude estimate of the increase in dislocation density  $\Delta\rho$  that occurs in the material by using the relation (D.Hull and D.J.Bacon,1965)

$$\sigma = \alpha Gb\rho^{1/2} \quad (2.9)$$

where  $\alpha$  is a material constant,  $G$  and  $b$  the shear modulus and Burgers vector respectively of the matrix. A model of the increase in dislocation density made by Arsenault and Shi (1986) for particulate reinforced MMCs is based on parallelepiped particles as shown in figure 2.9. Prismatic dislocations are assumed to be punched out of the faces of the particle due to a strain misfit proportional to the strain  $\epsilon$  given by equation 2.8, and yield to the result that the increase in dislocation density can be given by

$$\rho_i = K\alpha\Delta TV_i/bt(1-V_f) \quad (2.10)$$

where  $K$  is a geometrical constant,  $V$  is the volume fraction of the particles,  $b$  the Burgers vector of the matrix and  $t$  the

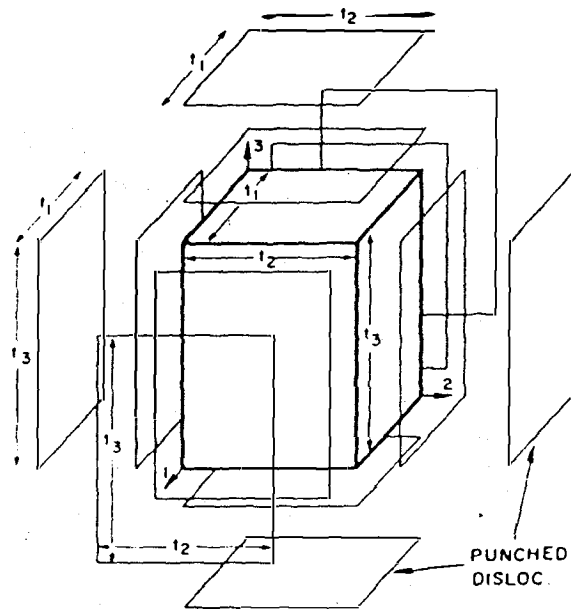


Figure 2.9 Diagram of a particle and several punched dislocations.

smallest length of the particle in figure 2.9. This model can therefore be used in conjunction with equation 2.9 to estimate the effect of the size and shape of the particles as well as their volume fraction of the increase on the yield stress of these particulate materials.

Both equations 2.9 and 2.10 predict that the dislocation densities created are isotropic and therefore testing in tension or compression should produce the same increase in flow stress  $\Delta\sigma$  for a given increase in dislocation density  $\Delta\rho$ .

## CHAPTER 3

### EXPERIMENTAL PROCEDURES

The objectives of this study included the determination of internal stresses in composites. These were determined by measurements of the Bauschinger effect and dimensional instability in different materials. In the first section this chapter will describe the various materials used and their preparation. A description of the mechanical testing procedures is then given in the second section.

#### **3.1 Materials:**

Three different materials were used in the course of this study; the aluminum alloy A-356, a composite made from the A-356 alloy containing SiC particulates and a composite of pure copper incorporating continuous tungsten fibres.

##### **3.1.1 Aluminum Based Materials:**

The aluminum composite material was a silicon rich casting alloy A-356 to which 20% volume fraction of silicon carbide (SiC) particles were added by the Duralcan process. The particles had an average particle size of 12  $\mu\text{m}$  and an

average aspect ratio of 2. The material was cast and extruded to 20 mm diameter bars. This composite, and the unreinforced A-356 matrix, were provided by Alcan International Ltd, Kingston Centre.

The chemical composition of the Al alloy and a micrograph of the composite are shown in table 3.1 and figure 3.1 respectively. All the specimens machined out of these materials were heat treated to a T61 condition as follows:

- Solution treating at 540°C for 4 hours
- Quenching in warm water
- Natural ageing for 16 hours
- Artificial ageing at 155°C for 9 hours
- Quenching in warm water

Due to this heat treatment, two precipitates were formed (see the Al-Si phase diagram, figure 3.2); a silicon rich one, between 4 and 5% volume fraction, having an average diameter of 1.5  $\mu\text{m}$  and an aspect ratio of 1 and  $\text{Mg}_2\text{Si}$ , a submicron precipitate.

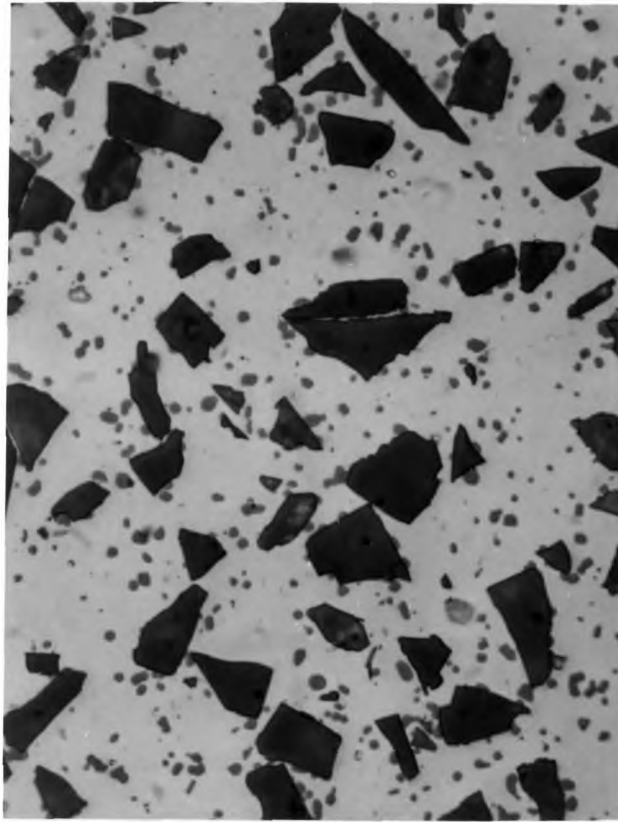
The distribution of the  $\text{SiC}_p$  is not perfectly homogeneous. The strength differential between the particles and the matrix can in itself be a cause of heterogeneous

Si	Mg	Mn	Cu	Others
7%	0.35%	0.05%	0.1%	0.5% max

Table 3.1 Alloying elements of A-356.

	Slope, mV/0.001"	Correlation
+25°C	0.084	0.99
-50°C	0.077	0.99

Table 3.2 Extensometer calibrations results.



12.5 um

Figure 3.1 Micrograph of the composite material Al-SiC.

stress states in the composite. The non-uniform distribution and the sharp edges of the  $\text{SiC}_p$  can furthermore increase this heterogeneity.

### 3.1.2 Copper-Tungsten Composite:

The preparation of this composite model was undertaken in order to have a model system with continuous fibres without the complication arising from a second set of particles (as with the Si and  $\text{Mg}_2\text{Si}$  precipitates in the Al particulate composite). The material and specimens were made by Warren Poole using 99.9% pure Cu shot melted into a cylindrical shape and infiltrating 99.98% pure tungsten fibres of 250  $\mu\text{m}$  diameter. The copper and the tungsten were obtained from Johnson Matthey Ltd..

The tungsten fibres were cleaned with a 10 molar solution of sodium hydroxide for 15 minutes, then rinsed with distilled water and finally with acetone for 15 minutes. The W fibres and the Cu were placed into a high density graphite mould as shown in figure 3.3.

An induction furnace was used to heat up the mould and its content to approximately  $1150^\circ\text{C}$  for 5 minutes to allow the Cu to melt and infiltrate in between the fibres. The mould was then slowly moved out of the induction coil to minimize

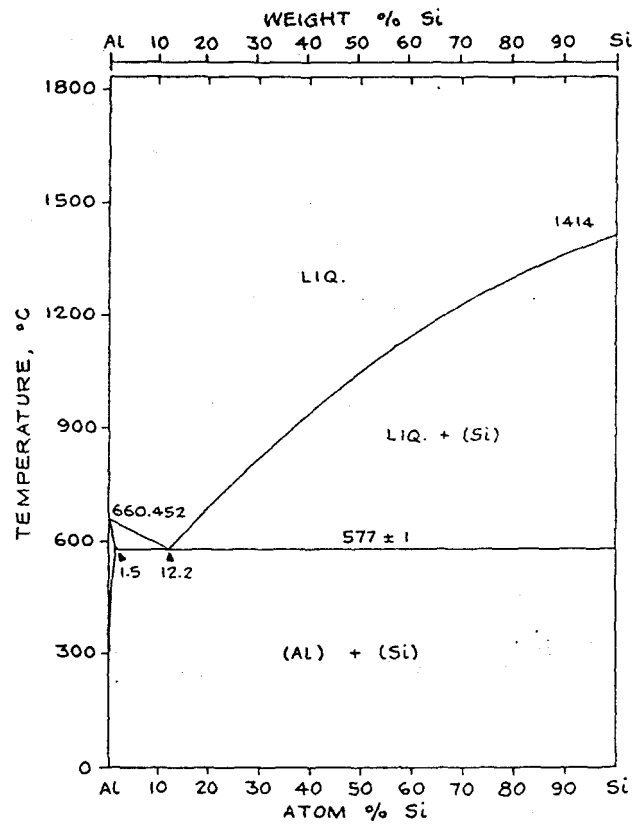


Figure 3.2 Aluminum-Silicon phase diagram

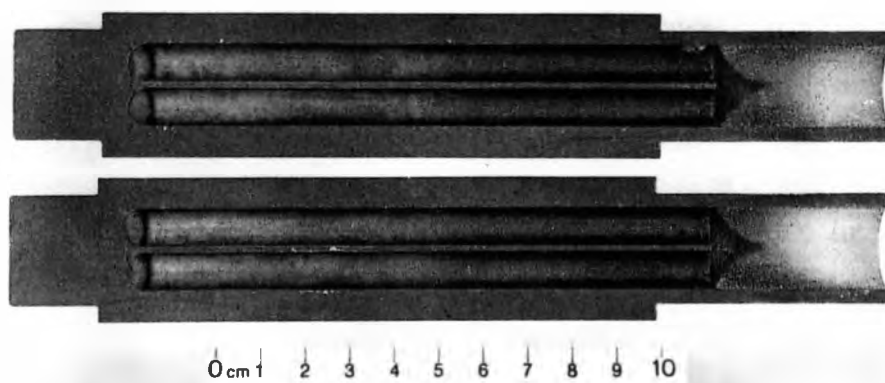


Figure 3.3 Graphite mould used in the making of Cu/W specimens.

porosity.

The composite specimens produced contained 10% volume fraction of continuous fibres dispersed randomly in the longitudinal direction. A cross section of a specimen can be seen in figure 3.4. The distribution of the fibres was fairly homogeneous although some fibre-free regions were present. Due to the slow cooling rate, the Cu solidified into a limited number of grains. A cross section might present 2 to 5 grains with diameters ranging approximately from 2 to 8 mm.

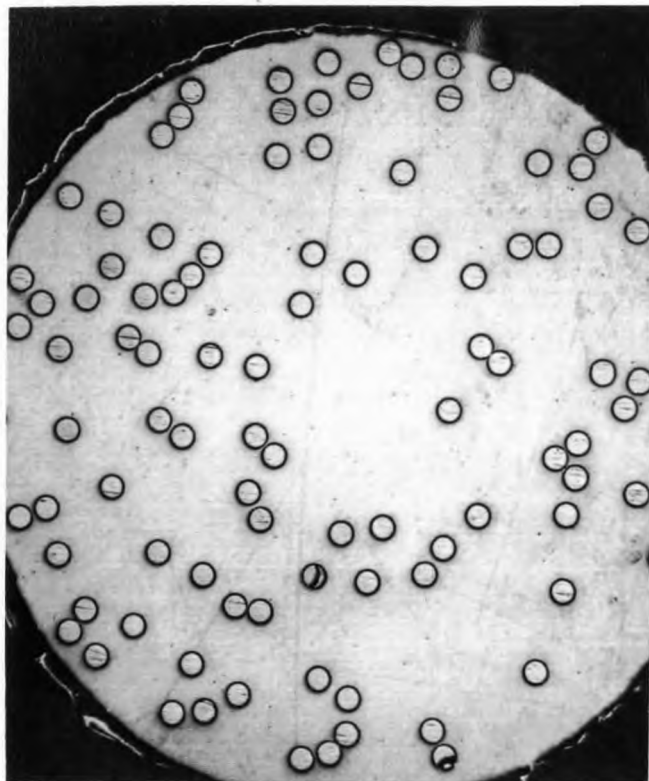
### **3.2 Mechanical Testing:**

#### **3.2.1 Introduction:**

Two types of experiments were performed with the materials described; Bauschinger experiments, which basically consisted in performing the first hysteresis loop of a low-cycle fatigue experiment, and a dimensional instability experiment. The Bauschinger experiment gives information on several parameters. The tension portion of the cycle can be considered as a simple tensile test. And the full hysteresis loop is a means to evaluate the development of the backstress in a material.

#### **3.2.2 Bauschinger Experiment:**

The measurements of the backstress, as previously



0.750 mm

Figure 3.4 Cross-section of a Cu/W specimen.

described in the literature review, were done on the Al/SiC composite and the unreinforced matrix. The cross-head speed used was always 0.05 "/minute which correspond to an average strain rate of 0.09"/"/minute assuming the specimens were the only component to deform during loading.

Two different testing temperatures, +25°C and -50°C, were used in order to measure the influence of the temperature on the deformation of the materials. The temperature of -50°C was obtained by cooling a container filled with methanol using liquid nitrogen. The nitrogen evaporated quickly from the surface of the alcohol leaving a cooler methanol. The temperature was continuously measured using a thermocouple and it was found to be very stable; the temperature could decrease by 1°C in about 4 minutes, which gave time to complete a test. To ensure the specimens were at the desired temperature, the specimen and the apparatus used were immersed and maintained in the -50°C methanol bath for a minimum of 20 minutes prior to testing. The temperature was adjusted by pouring liquid nitrogen into the bath.

The specially designed rig described by Watt (1966) which was used allowed testing to be done on an Instron TTC-L floor model tensile tester equipped with a tensile-compression FR load cell of a capacity of 10 000 lbf. A partial drawing of the rig is shown in figure 3.5 and the set-up on the Instron

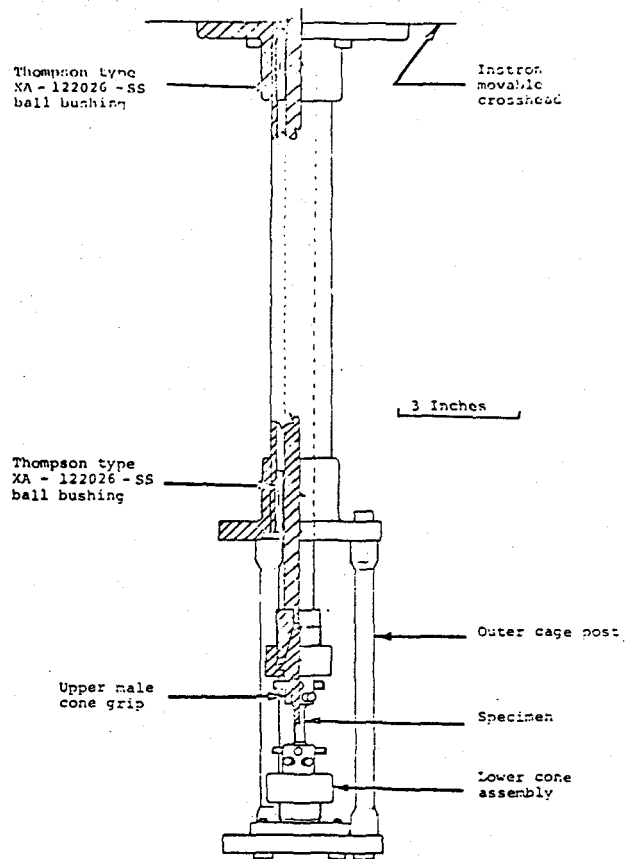


Figure 3.5 Partial drawing of the Bauschinger rig  
(from Watt, 1968).

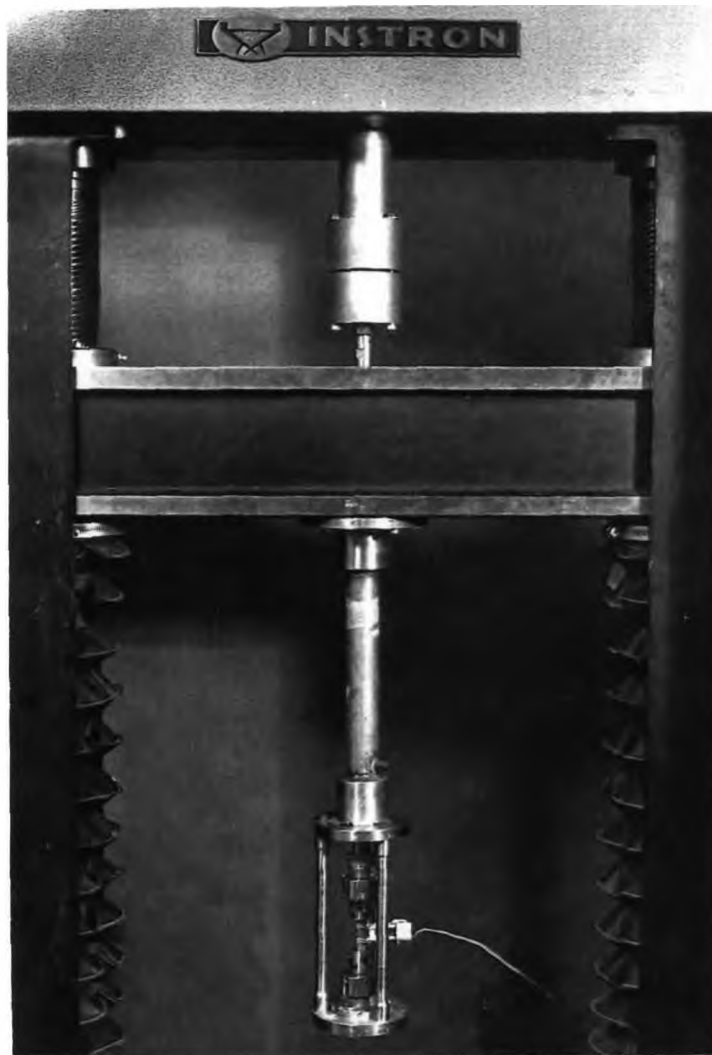


Figure 3.6 Set-up of the Bauschinger rig on the Instron tension compression tester.

is shown in figure 3.6.

The rig was attached under the cross-head of the Instron. A shaft was fixed to a coupling device shown in figure 3.6 which was itself attached to the load cell. This coupling allowed a rigid fit between the shaft and the load cell and three screws were used for adjusting any misalignment between the two.

In order to avoid the buckling of the specimens during the loading in compression, the specimens were designed with the largest diameter possible at the gauge section and the shortest gauge length possible ( $\text{length/diameter}=2.9$ ). Care also had to be taken to avoid slipping of the specimens into the grips since they were held by friction. As a result the specimen specifications in figure 3.7 were used for the Al/SiC<sub>p</sub> composite and the unreinforced Al matrix. It consists of a tubular shaped tensile specimen of 22 mm gauge length with 7 mm exterior diameter and 3.125 mm interior diameter at the gauge section. The reduced cross section helped limit the load to lower levels during testing.

The specimens were held in the grips using eight screws in each grip. An alignment rig shown in figure 3.8 was used to ensure accurate set-up of the specimens. One end of

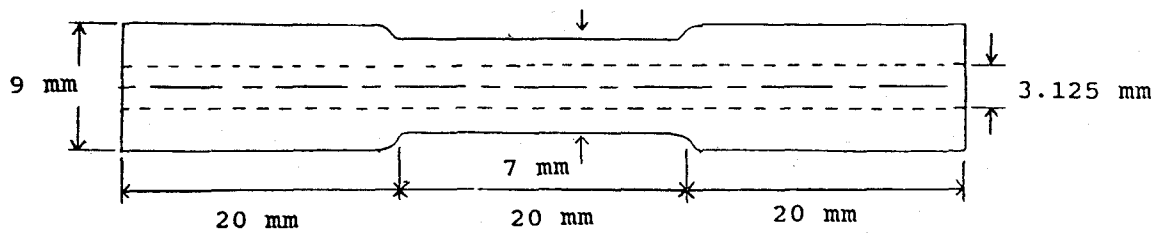


Figure 3.7 Specifications for the Bauschinger experiments specimens.



Figure 3.8 Alignment rig used to set-up the specimens in the grips.

the specimen was inserted in a grip previously screwed on the base of the rig. An alignment post with a sharp end served to show any misalignment. The eight screws were slowly adjusted while rotating the grip in order to detect any misalignment. After the first end had been fixed, the grip was removed, the other grip fixed on the base and the free end of the specimen placed in that grip.

A careful alignment and tight set-up of a specimen in the grips usually took about 30 minutes and was important in order to avoid buckling or slipping of the specimens relative to the grip. A bi-directional Mitutoyo travelling microscope was used to measure the misalignment resulting from the set-up procedure and showed that the specimens were misaligned by a maximum of 60  $\mu\text{m}$  laterally. A misalignment of this order, considering the distance of approximately 25 mm between the grips, is equivalent to less than  $0.15^\circ$ . No buckling of such a misaligned specimen was observed.

The grips and the specimen were then tightly set in the Bauschinger rig (figure 3.9). As a result and due to the overall stiffness of the rig, no pause occurred during the load transfer from tension to compression.

### 3.2.3 Stress-Strain Measurement:

The load was, as mentioned before, measured using an

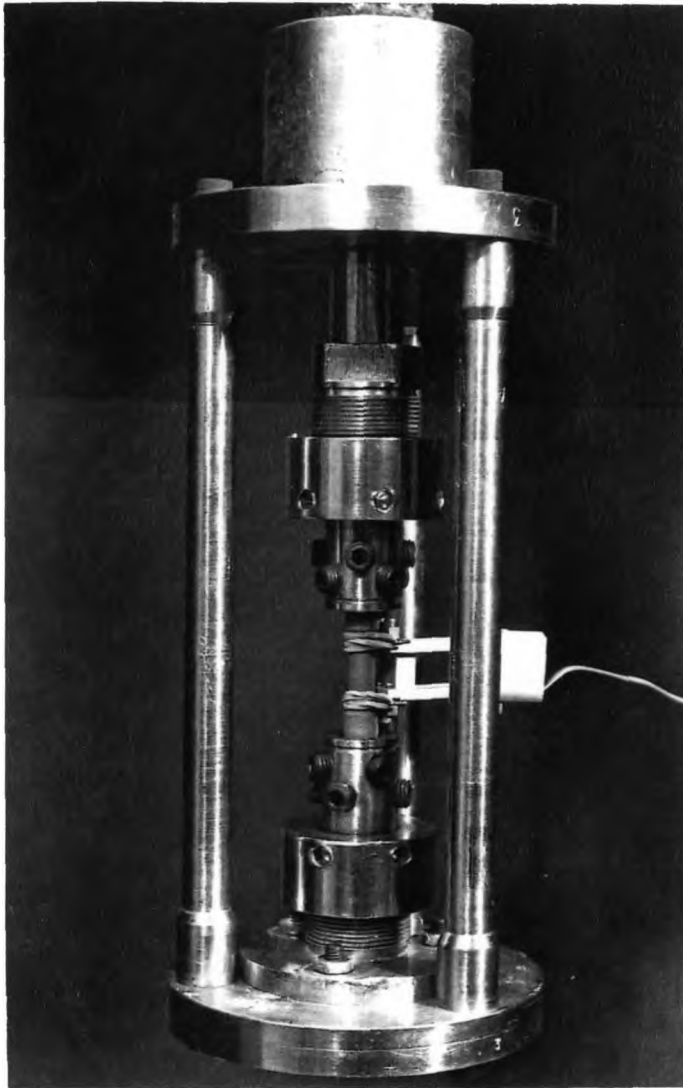


Figure 3.9 Close-up at the Bauschinger rig showing a specimen in the grips and the extensometer used.

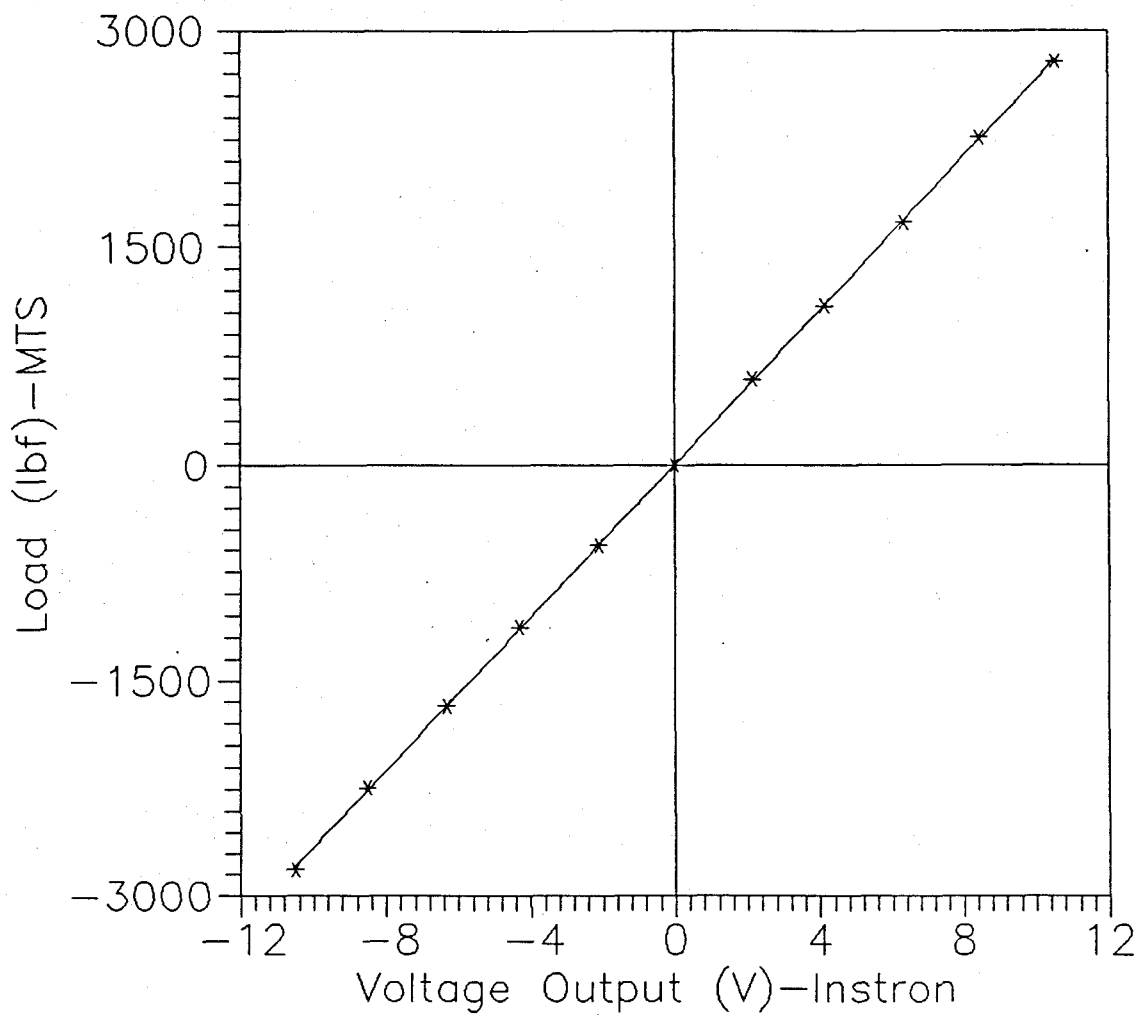


Figure 3.10 Load cell calibration curve.

Instron FR load cell. An amplifier was used to process the signal and the final recording was done on a Philips X-Y recorder. A calibration of the load cell in both tension and compression was done on an MTS tensile machine using a calibrated MTS load cell. A plot of the calibration is shown in figure 3.10. A linear regression analysis gave a slope of 0.00377 volt/0.001" with a correlation of 0.99.

To ensure accurate measurement of the strain, an extensometer specially made with a gauge length of 14 mm was always used as shown in figure 3.9. The signal from the extensometer was amplified and plotted by the recorder. Several calibrations were made (figure 3.11 and 3.12) and the results are shown in table 3.2. The plastic strain levels involved in the Bauschinger experiments ranged from 0.0011 (0.11%) to 0.021 (2.1%).

#### 3.2.4 Dimensional Instability Experiment:

The Al/SiC<sub>p</sub> composite and the unreinforced Al matrix were used in an experiment in order to evaluate the dimensional change that can occur when internal stresses are thermally allowed to relax.

The experiment first consisted in deforming plastically the specimens by different amounts of strain. The

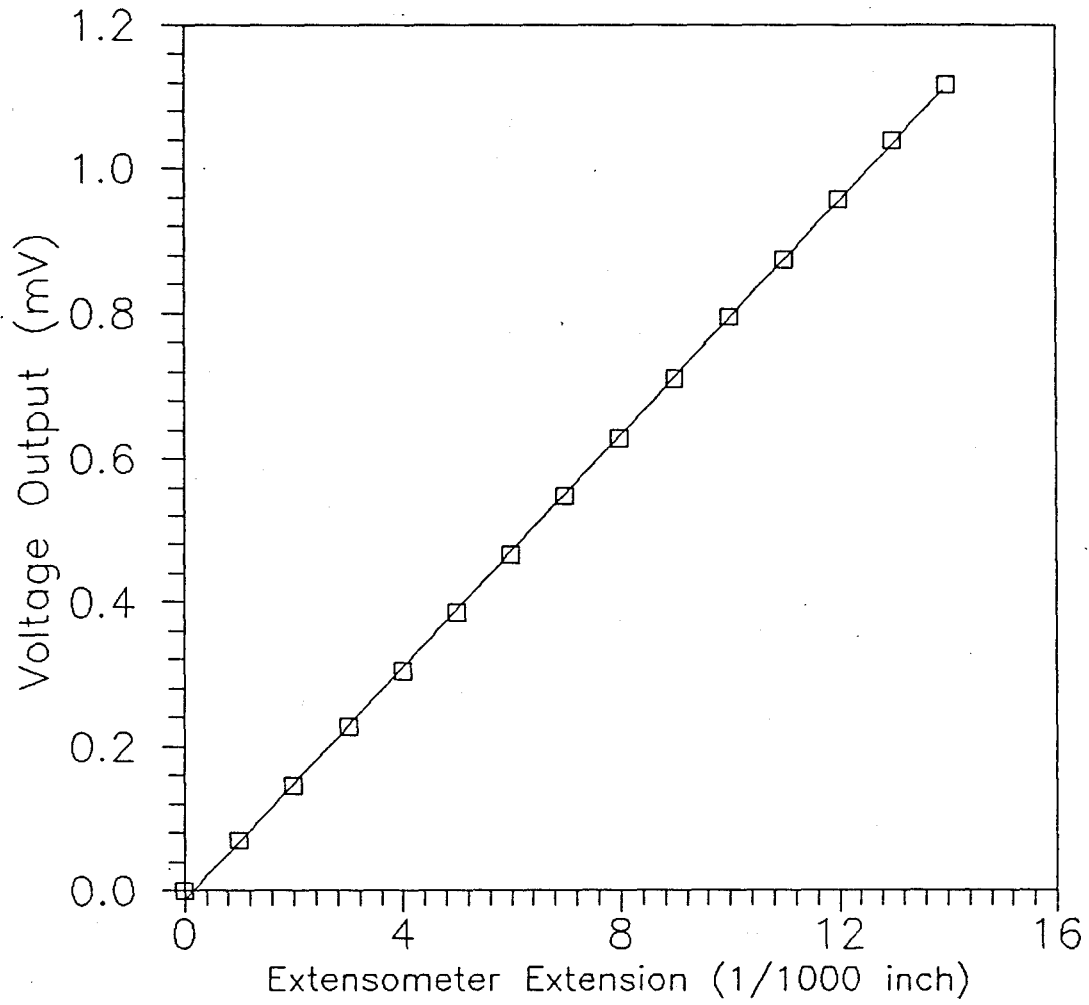


Figure 3.11 Extensometer calibration curve at +25°C.

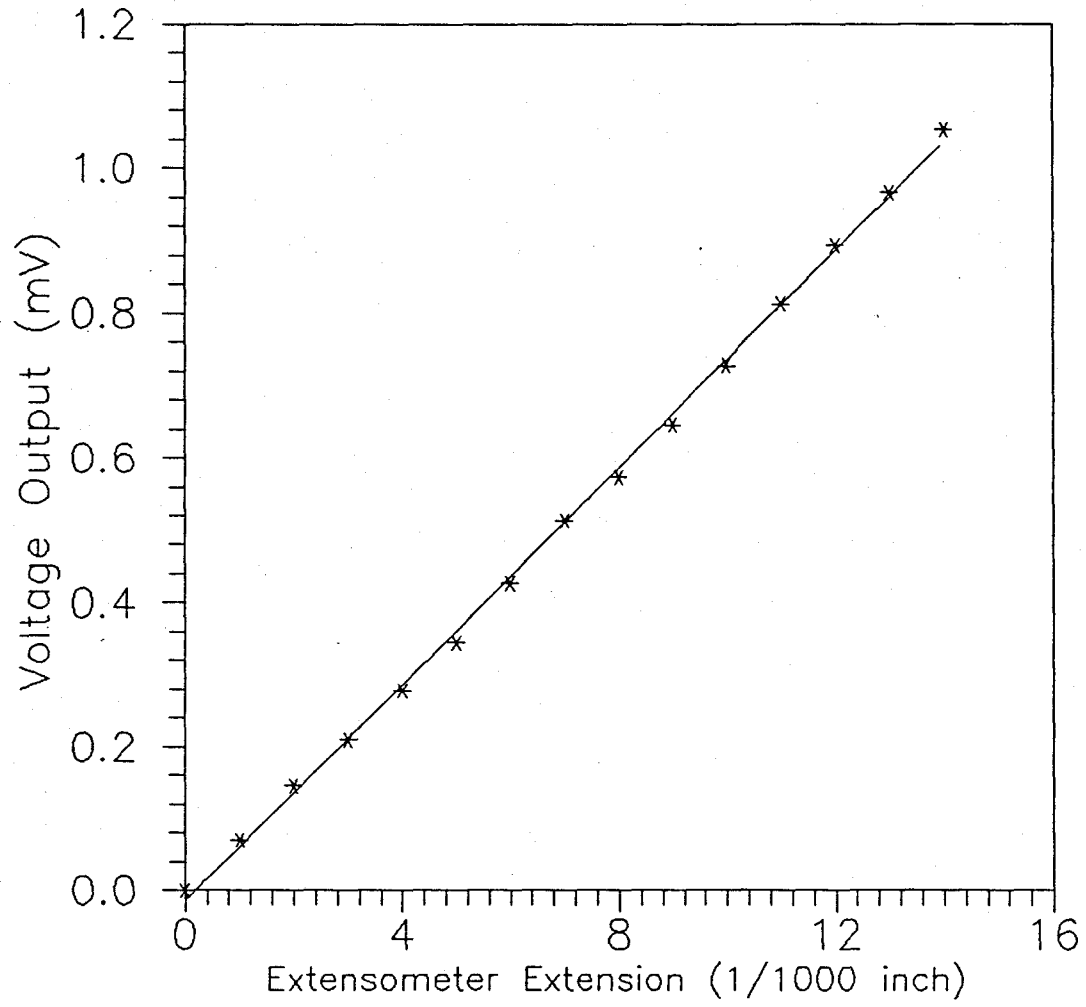


Figure 3.12 Extensometer calibration curve at  $-50^{\circ}\text{C}$ .

initial thickness of the specimens ranged from 6 to 8 mm. The compressions were done at +25°C, -50°C and -196°C. Different temperatures were chosen to determine the effects of the testing temperature on the magnitude of internal stresses stored in the materials.

The compressions, in the range of 0.04 (4%) to 0.24 (24%) were measured by taking the difference in thickness before and after compression and were done using the Bauschinger rig described earlier. The grips were replaced by two flat ended cylinders shown in figure 3.13 with a specimen.

After the compression, the thickness of the specimens were measured carefully using a micrometer. Those measurements readings were accurate within  $\pm 2 \text{ um}$  or a strain of approximately  $\pm 2 \times 10^{-4}$ . The specimens were then kept for 24 hours at three different temperatures: 25°C, +155°C and +250°C. The final thickness of the specimens were measured after they had cooled down from their respective heating temperature.

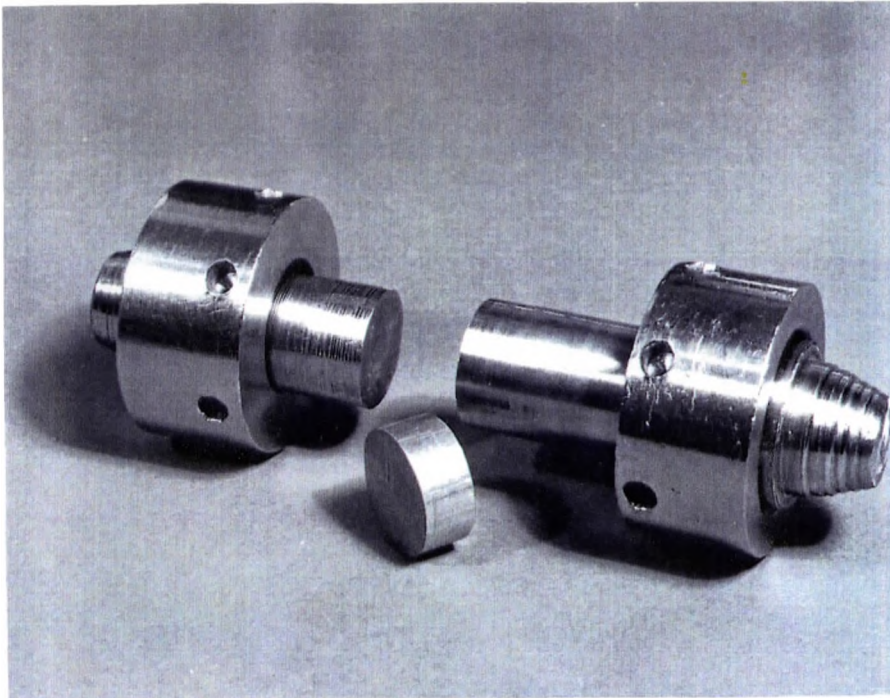


Figure 3.13 Specimen used for the dimensional instability experiments and the flat ended cylinders used for the compression.

## CHAPTER 4

### RESULTS

#### 4.1 Introduction:

The transition from elastic to plastic behaviour in composites is complex and was introduced on a macroscopic and microscopic basis in the literature review. In the course of monotonic loading of a specimen after this transition the plastic deformation can be simply viewed using a microscopic model in which the mobile dislocations accumulate at obstacles such as second phases. As a result these obstacles are stressed (see illustration in figure 2.6b). With increasing plastic strain a critical stress can be reached at which the second phase is cut or fractured and the resultant average elastic stress in the particle lowered. The process of building up elastic stresses then starts again on the fractured particles.

These build-ups and releases of internal elastic stresses occur at different rates at different locations in the material as it is deformed. Therefore the magnitude of residual stresses which can be found in a material can vary as

a function of its level of deformation. The internal stresses can be measured by their effects on subsequent mechanical testing. That is the material, upon unloading, has a memory of its previous deformation; the number and location of the dislocations as well as the damage incurred reflect the mechanical history of the material.

Due to this mechanical memory, a change in the direction of deformation can reveal information on the extent to which internal stresses have built up and the damage, or relaxation of those stresses, developed. The simplest change of deformation path is, as used in this work, the direction opposite to the previous deformation: compression loading after tension (see figure 2.7 in literature review). The initial work hardening, yield stress and flow in the reverse loading direction are influenced by the level of internal stress in a material after the deformation in the forward direction.

#### **4.2 Mechanical Response of the Unreinforced and Composite**

##### **Materials:**

This section will present the results obtained from tensile and Bauschinger testings for both the unreinforced and particulate composite materials. The averages values of the modulus and offset stresses at strains of  $10^{-4}$  and  $10^{-3}$  are

Specimen #	Testing Conditions
16	Unreinforced; Tested at R.T.; Tension
17	" " " " "
18	" " " " "
20	" " " " "
21	" " " " "
44	" " " " "
23	Unreinforced; Tested at -50°C; Tension
45	" " " " "
47	" " " " "
48	" " " " "
49	" " " " "
67	" " " " "
68	" " " " "
69	" " " " "
24	Composite; Tested at R.T.; Tension
25	" " " " "
27	" " " " "
28	" " " " "
29	" " " " "
32	" " " " "
33	" " " " "
35	" " " " "
73	" " " " "
74	" " " " "

Table 4.1 Material and testing conditions of each specimen used for the Bauschinger experiments.

Specimen #	Testing Conditions
37	Composite; Tested at -50°C; Tension
38	" " " " "
39	" " " " "
41	" " " " "
42	" " " " "
78	Comp.; Thermally Cycled; Tested at R.T.; Tension
79	" " " " " " Compr.
64	Unr.; Thermally Cycled; Tested at R.T.; Tension
65	" " " " " " Compr.
60	Unreinforced; Tested at R.T.; Compression
61	" " " " "
62	" " " " "
66	Unreinforced; Tested at -50°C; Compression
75	Composite; Tested at R.T.; Compression
76	" " " " "
77	" " " " "

Table 4.1 (continued)

	$\sigma_{f10-4}$ MPa	$\sigma_{f10-3}$ MPa	$\sigma_{r10-4}$ MPa	$\sigma_{r10-3}$ MPa	$\sigma_F$ MPa	$\epsilon_p$	E GPa
16	159	199	76	177	247	0.0102	71
17	166	214	47	168	259	0.0154	74
18	167	211	89	185	236	0.0055	72
20	168	215	93	193	237	0.0041	76
21	177	213	139	211	217	0.0014	72
23	156	211	90	187	248	0.0061	75
24	199	289	31	192	362	0.0098	120
25	199	270	47	181	334	0.0148	103
27	212	297	81	227	340	0.004	121
28	237	304	43	221	355	0.0055	114
29	219	292	106	255	304	0.0017	114
32	227	300	52	225	362	0.0074	112
33	218	296	98	222	374	0.0156	113
35	227	297	50	225	350	0.0060	114
37	212	307	31	212	378	0.0059	113
38	191	303	148	272	307	0.0011	120
39	192	301	0	194	388	0.0083	119
41	191	307	0	204	393	0.0103	105
42	206	305	16	193	399	0.0173	111
44	171	209	130	205	224	0.0028	73
45	165	219	0	167	276	0.011	76
47	180	-	91	-	216	0.006	80
48	171	218	-16	192	275	0.0136	76
49	167	223	56	179	294	0.021	78

Table 4.2 Mechanical response of each specimen used in the Bauschinger experiments.

	$\sigma_{n0-4}$ MPa	$\sigma_{n0-3}$ MPa	$\sigma_{r10-4}$ MPa	$\sigma_{r10-3}$ MPa	$\sigma_f$	$\epsilon_p$	E
60	127	197	55	153	240	0.0115	76
61	161	196	0	149	271	0.0157	72
62	148	194	56	158	224	0.0064	76
64	150	198	89	178	230	0.0056	89
65	164	218	56	172	248	0.0059	87
66	176	230	23	178	289	0.013	84
67	163	212	26	157	267	0.013	90
68	161	221	0	142	276	0.017	103
69	155	211	83	191	250	0.006	97
73	196	254	47	179	320	0.017	122
74	212	267	36	160	323	0.0124	126
75	-*	244	27	199	344	0.0114	-*
76	-*	289	38	155	289	0.0056	-*
77	-*	247	67	211	364	0.0166	-*
78	234	302	78	224	347	0.0064	125
79	203	302	63	233	368	0.0062	125

Table 4.2 (continued)

	$\sigma_{f10}^{-4}$ MPa	$\sigma_{f10}^{-3}$ MPa	E GPa
Unreinforced Tested at R.T. Tension	167 (8)	210 (5)	73 (2)
Unreinforced Tested at -50°C Tension	165 (6)	218 (4)	76 (1)
Composite Tested at R.T. Tension	217 (12)	293 (10)	114 (5)
Composite Tested at -50°C Tension	198 (9)	305 (2)	114 (6)
Unreinforced Tested at R.T. Compression	145 (17)	196 (2)	75 (2)
Composite Tested at R.T. Compression	--	260 (25)	--

Table 4.3 Mechanical response averaged per testing conditions and material. Standard deviation in brackets.

	Average (HRF)	Std.Dev.
Unreinforced, batch #1	86	0.78
" " #2	85.3	0.99
" " #3	84	0.93
Composite, batch #1	94.7	0.89
" " #2	95.2	0.39
" " #3	94.4	0.79

Table 4.4 Hardness results obtained after T61 heat treatment.

shown in table 4.3 for the materials subjected to a variety of testing conditions described in table 4.1. The hysteresis loops from these tests are shown in figures 4.1 to 4.4

It can be seen with figure 4.5 and 4.6 that the permanent softening, as defined in the literature review, cannot be measured because the curves intersect instead of becoming parallel. The backstress was therefore calculated at a given reverse strain using the following formulation

$$\sigma_B = (\sigma_F - \sigma_R)/2$$

as introduced in the literature review.  $\sigma_F$  is the forward stress prior to the reversal of the loading direction and  $\sigma_R$  the yield stress in the reverse direction. The latter term was evaluated using  $10^{-4}$  and  $10^{-3}$  offset strain and since these  $\sigma_R$  are larger at  $10^{-3}$  the backstress calculation results in lower values for  $10^{-3}$  than  $10^{-4}$ . All the values for  $\sigma_F$  and  $\sigma_R$  are presented in table 4.2 and the backstress results in figures 4.7 to 4.10.

From these curves it can be seen that the composite material has different relaxation mechanisms when testing at R.T. compared to  $-50^\circ\text{C}$ . Testing at  $-50^\circ\text{C}$  brought the saturation level of backstress to 200 MPa, using the  $10^{-4}$

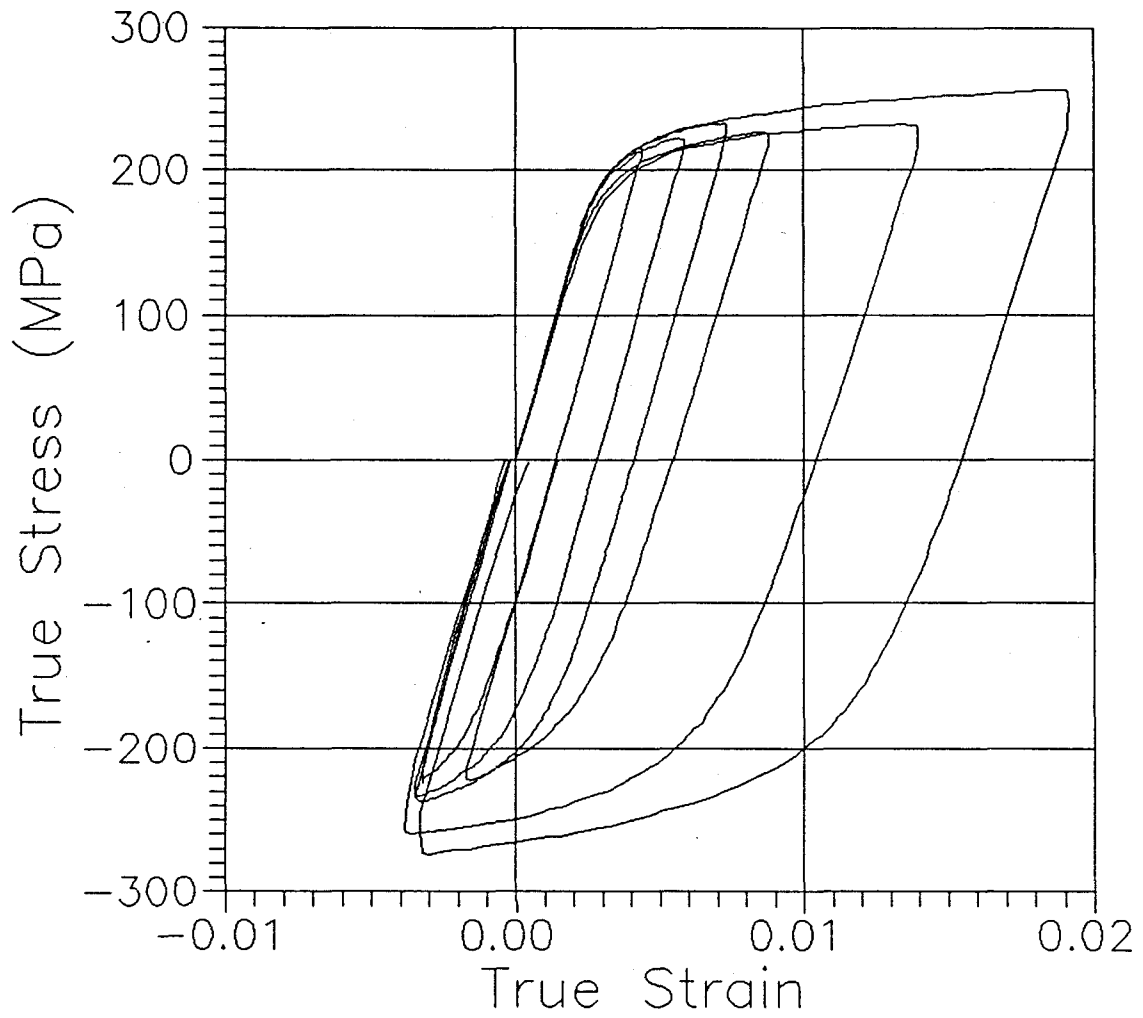


Figure 4.1 Hysteresis loops for the unreinforced material, R.T.. Tension first testing only.

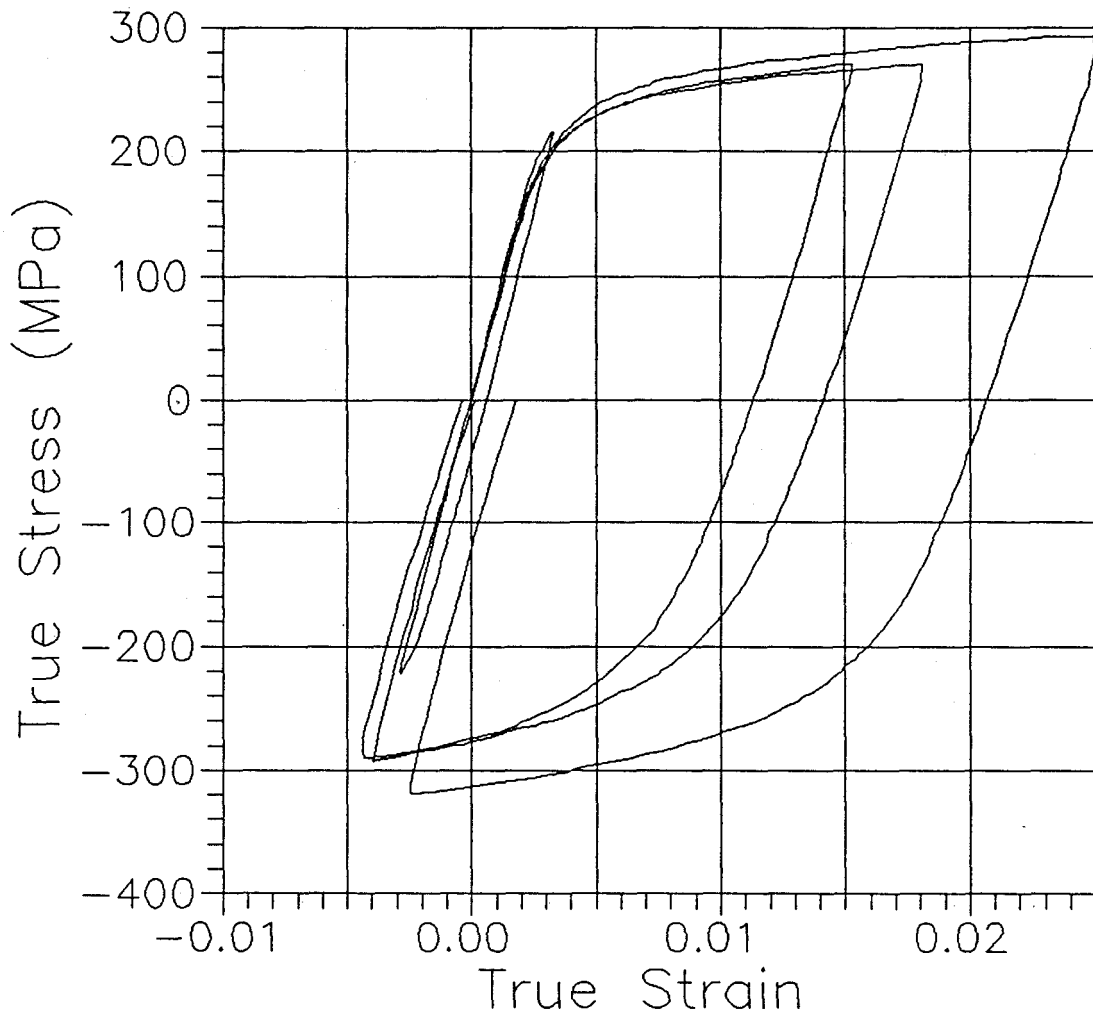


Figure 4.2 Hysteresis loops for the unreinforced material,  $-50^{\circ}\text{C}$ . Tension first testing only.

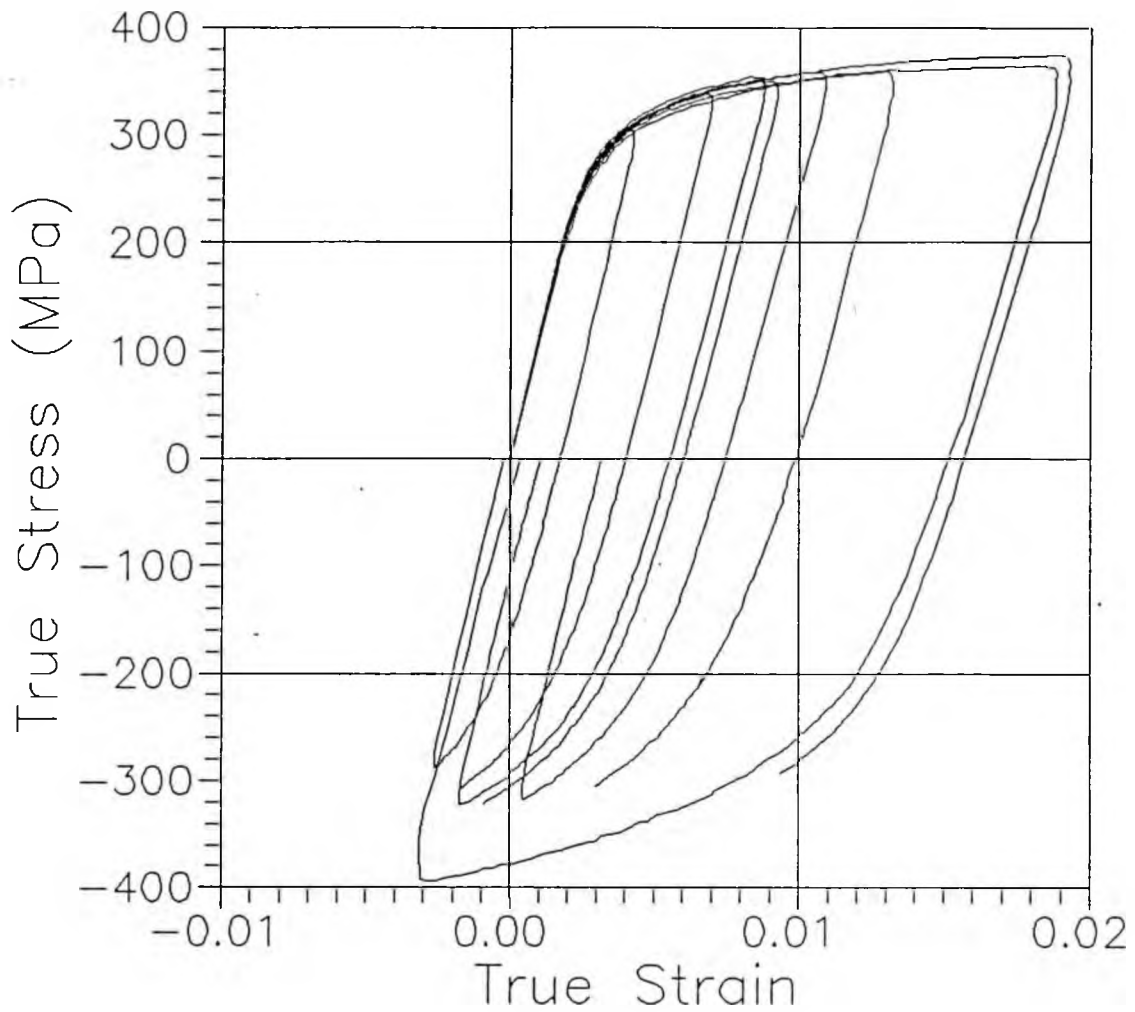


Figure 4.3 Hysteresis loops for the particulate composite material, R.T.. Tension first testing only.

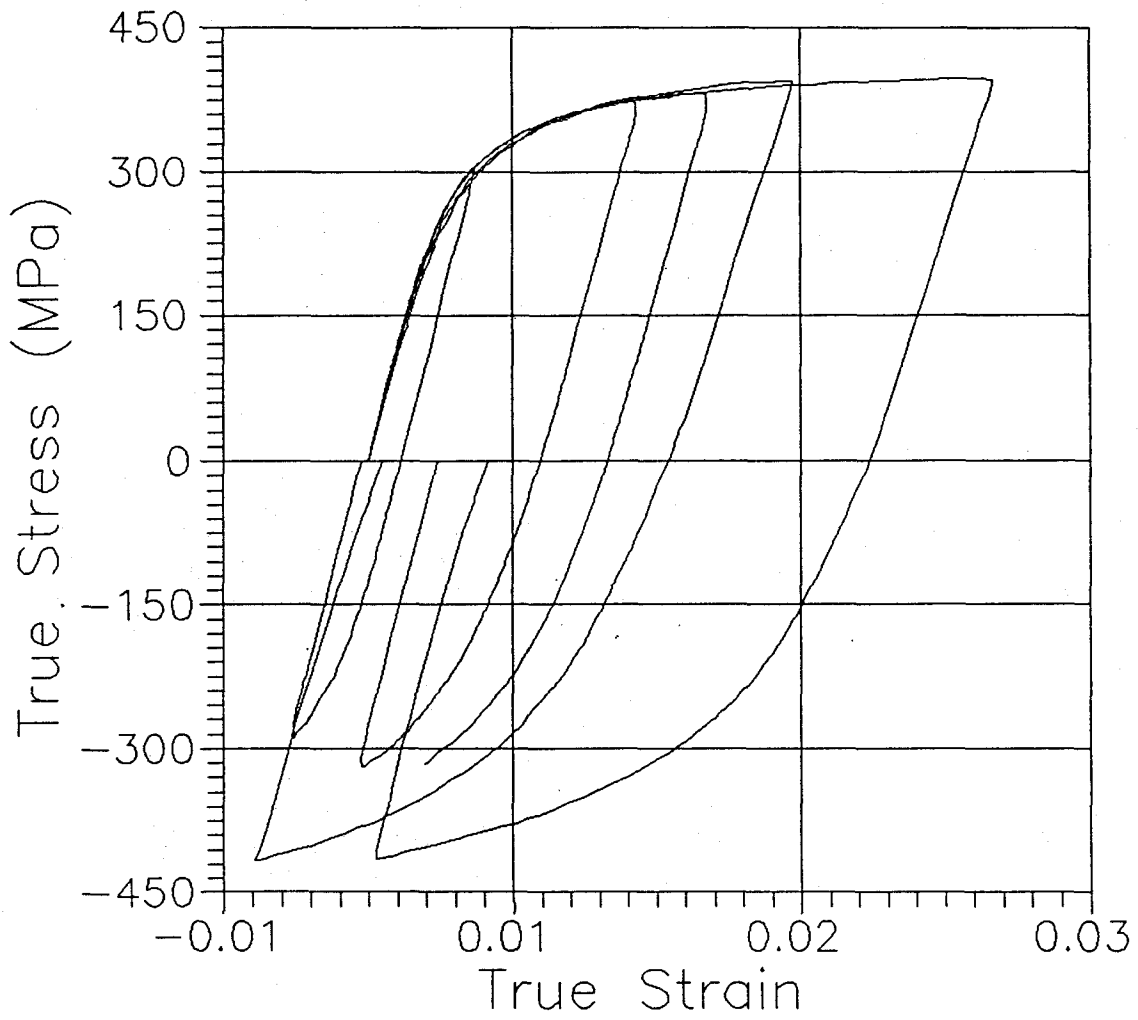


Figure 4.4 Hysteresis loops for the particulate composite material,  $-50^{\circ}\text{C}$ . Tension first testing only.

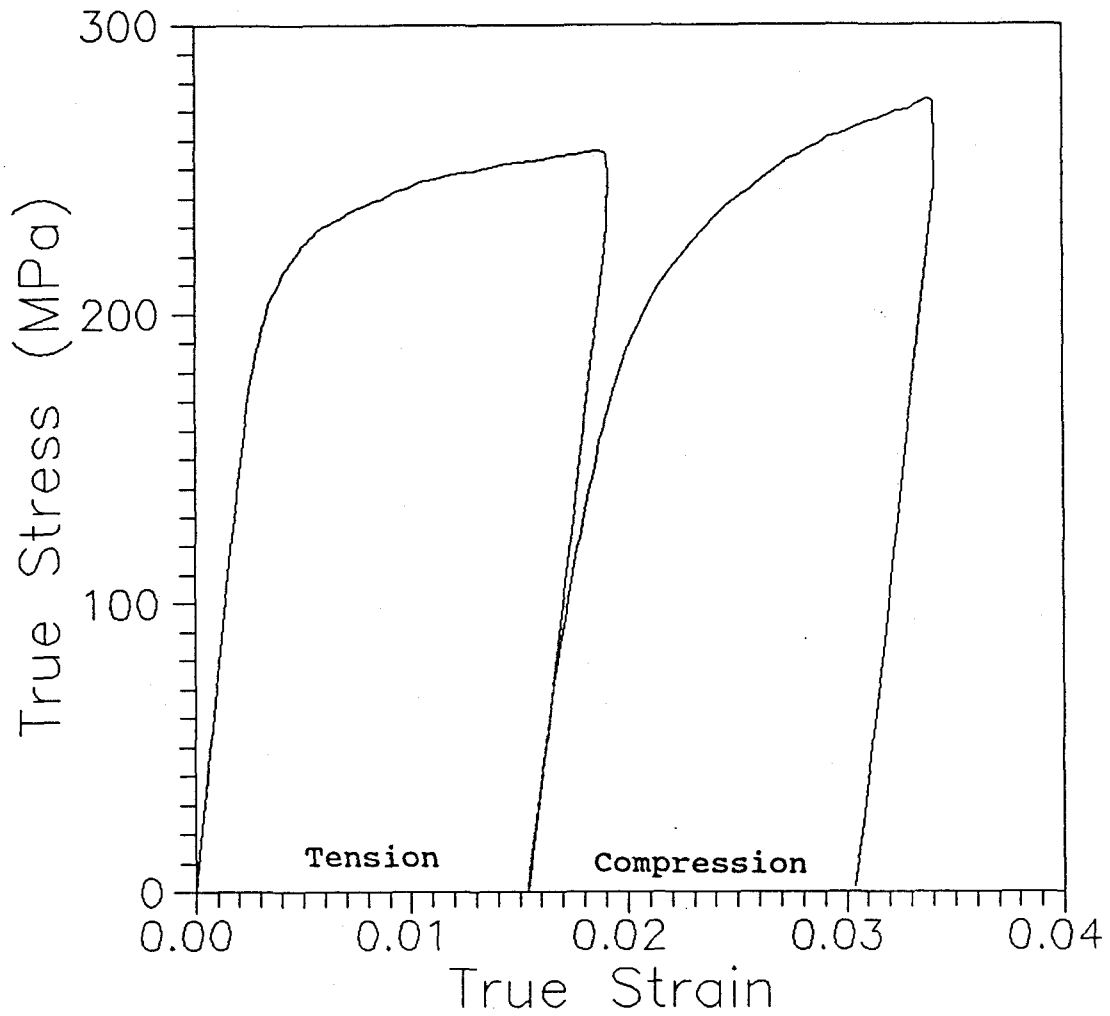


Figure 4.5 Typical Bauschinger experiment result for the unreinforced material showing no measurable permanent softening.

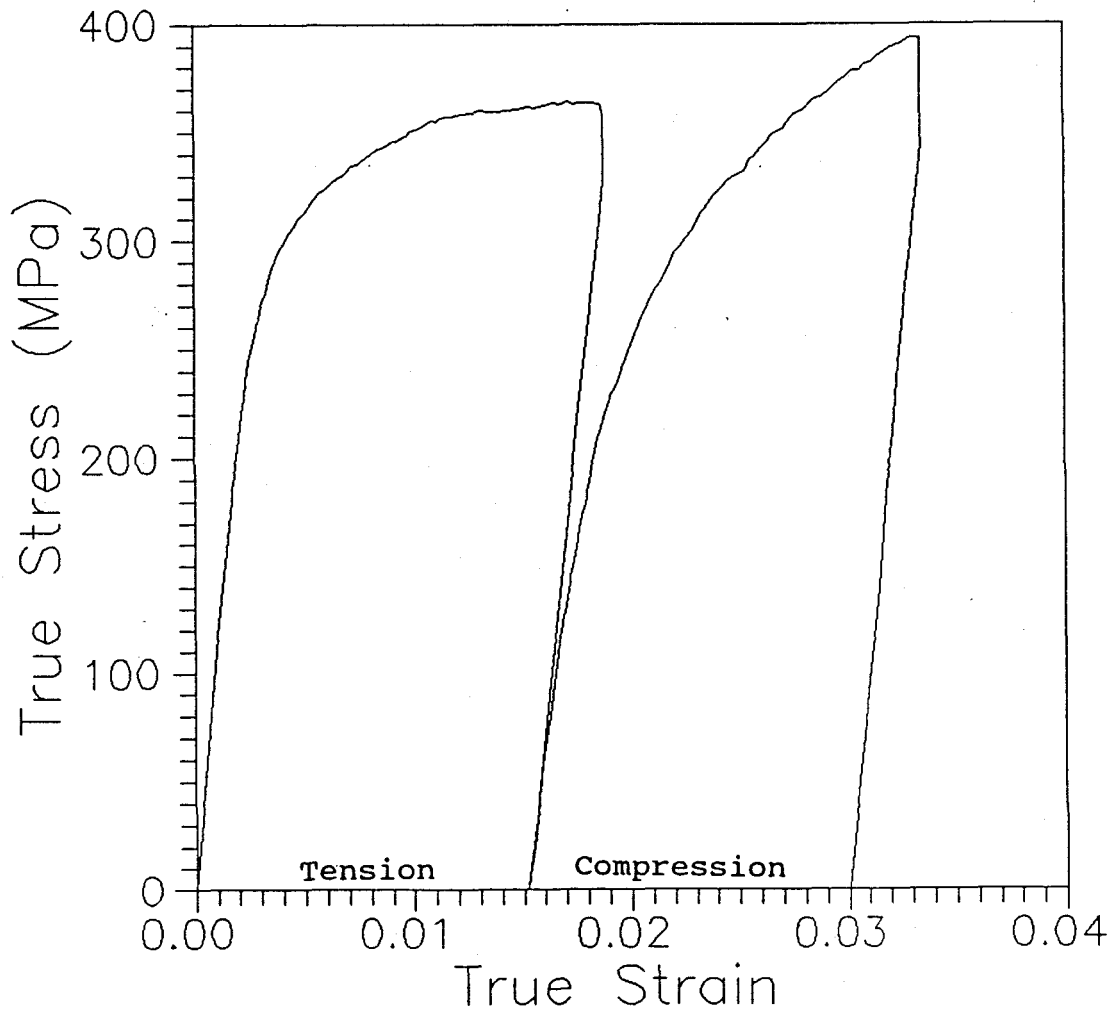


Figure 4.6 Typical Bauschinger experiment result for the particulate composite material showing no measurable permanent softening.

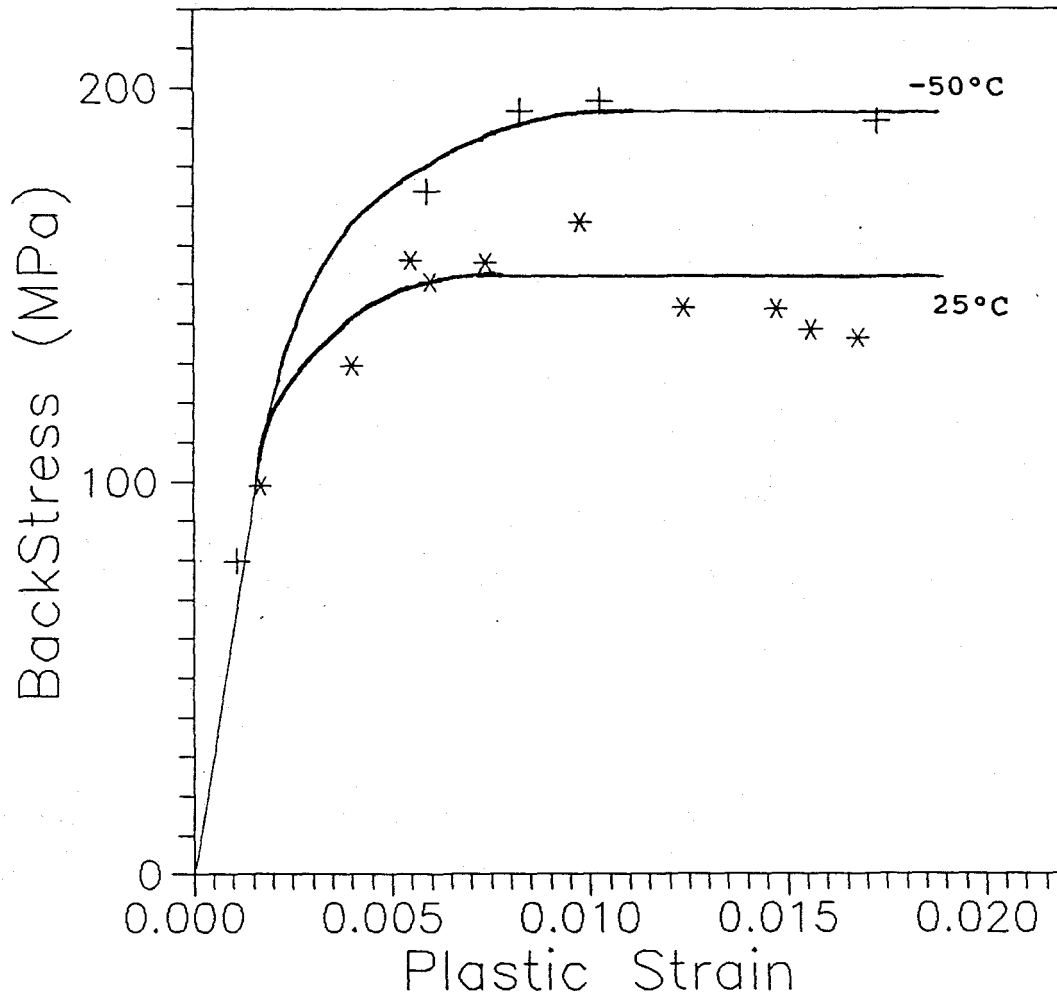


Figure 4.7 Backstress measurement results for the particulate composite material,  $10^{-4}$  yield offset.

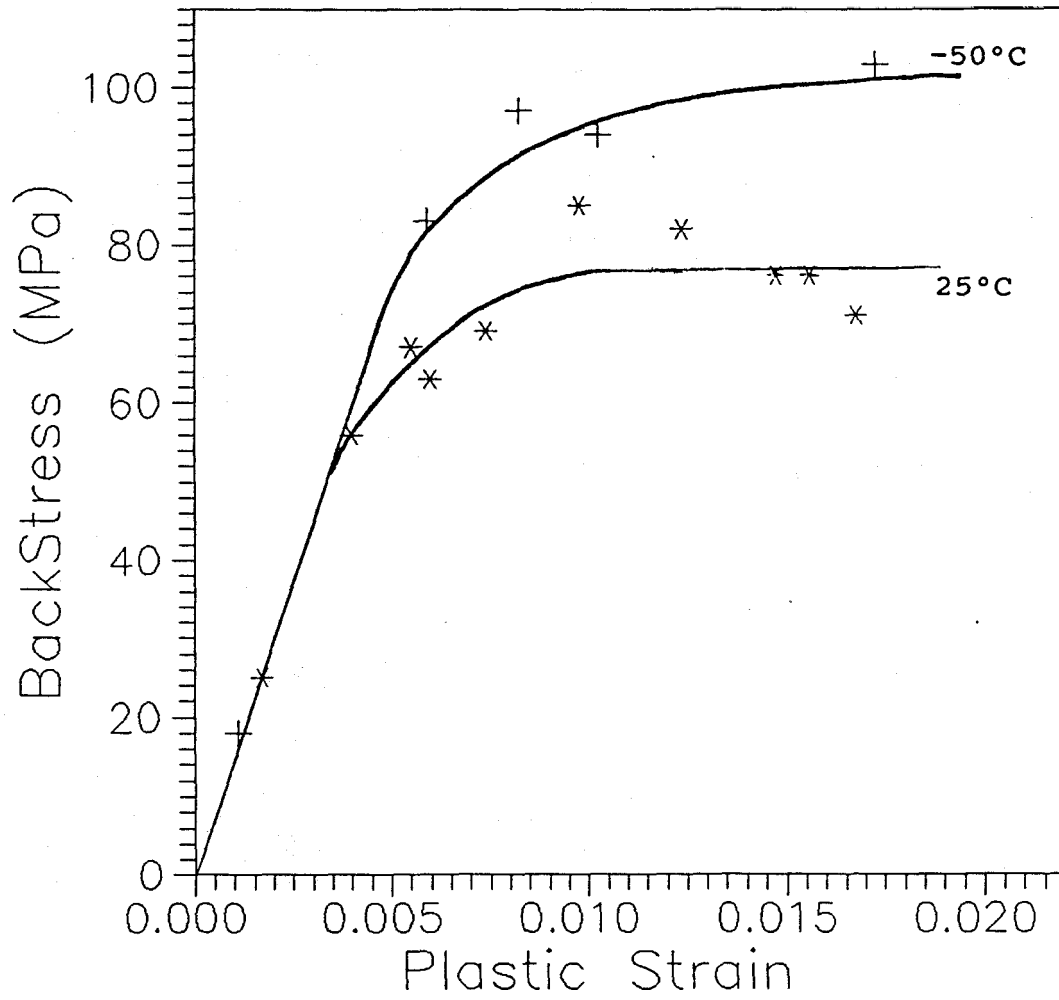


Figure 4.8 Backstress measurement results for the particulate composite material,  $10^{-3}$  yield offset.

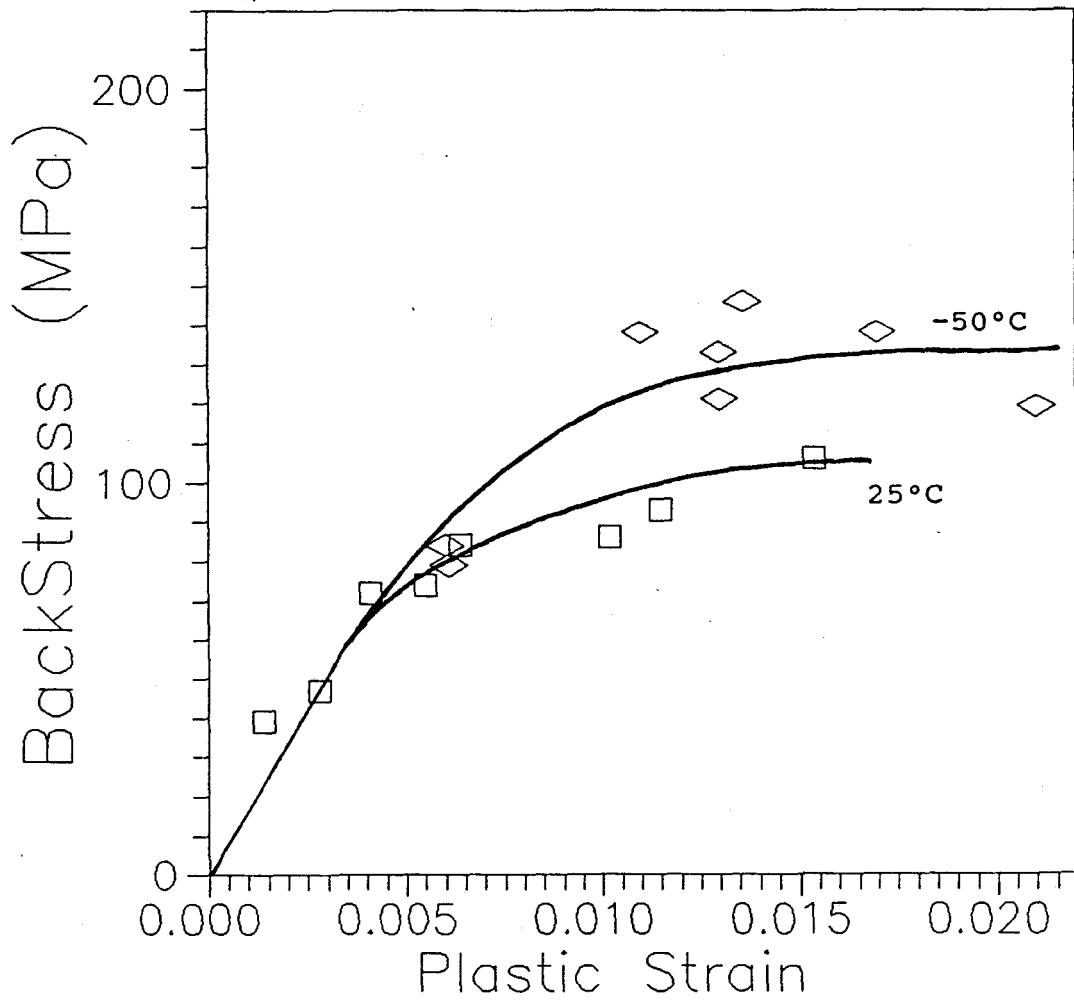


Figure 4.9 Backstress measurement results for the unreinforced material,  $10^{-4}$  yield offset.

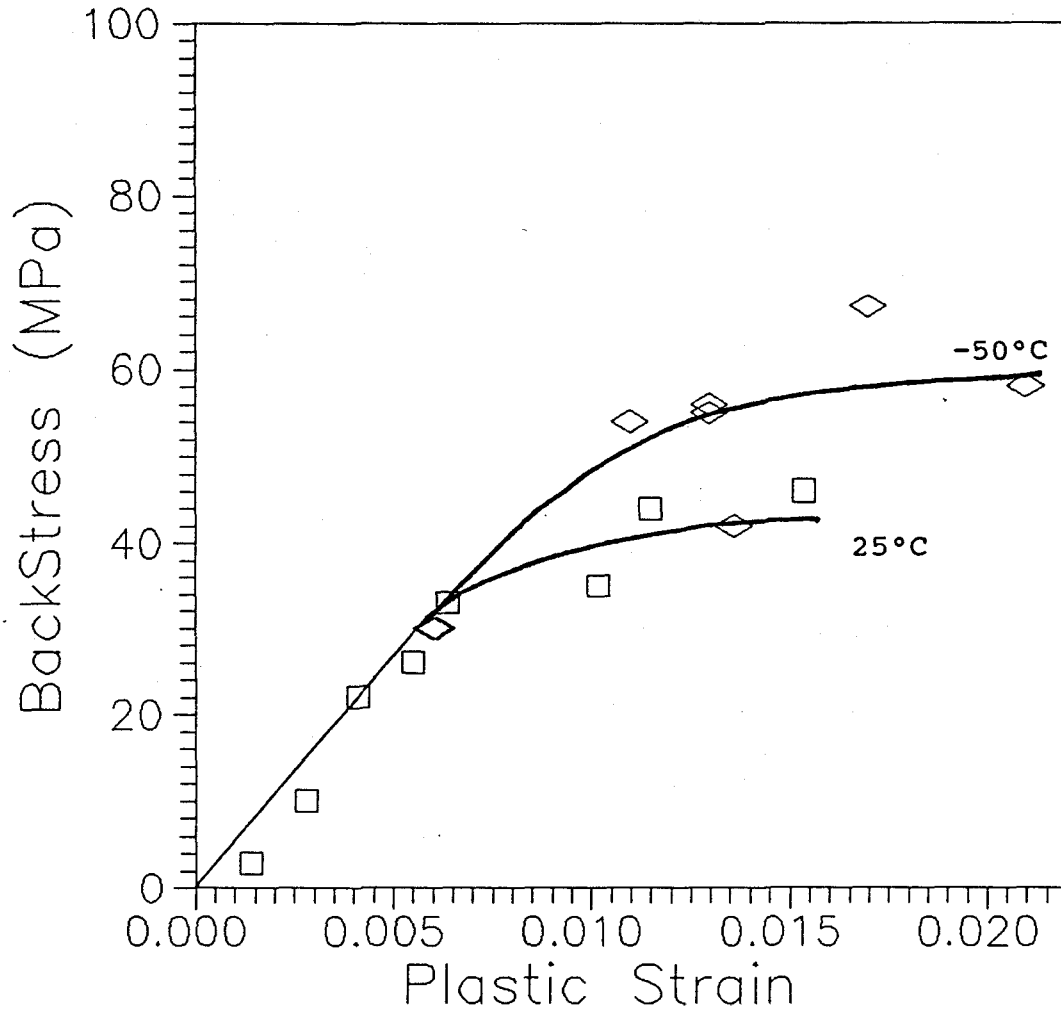


Figure 4.10 Backstress measurement results for the unreinforced material,  $10^{-3}$  yield offset.

offset, or 100 MPa using  $10^{-3}$  offset. The maximum backstress is reached after only 0.9% plastic deformation. The initial rate of increase of the backstress, which is related to the volume fraction of the second phase, is in the composite 50 GPa ( $10^{-4}=\epsilon_p$ ) and only 17 GPa ( $10^{-4}=\epsilon_p$ ) in the unreinforced matrix. These measurements were made assuming that no internal stresses were initially present in the materials prior to testing (see discussion).

The level of internal stresses in the unreinforced material is as expected less than in the composite. The backstress reaches about 130 MPa ( $10^{-4}=\epsilon_p$ ) when tested at  $-50^\circ\text{C}$  and 95 MPa ( $10^{-4}=\epsilon_p$ ) at R.T.. As in the case of the composite, the backstress results are reduced by half with the use of  $10^{-3}$  offset.

Some of the results presented in these graphs were taken from tests done starting in compression, that is were performed in the reverse direction first (compression) and then in tension. (In table 4.2, the forward results can therefore be for tests starting in tension or compression. Reference to table 4.1 indicates the initial loading direction of each of the specimens.). The purpose of doing the hysteresis loop starting in compression was to verify if the build-up of internal stresses reached the same magnitude for

the same plastic deformation. The results obtained are in agreement with the ones obtained in "tension first" tests. Figure 4.11 however shows for the composite material that the stress strain curves do have some differences. For clarity the compression curves were reflected into the first quadrant so a comparison can be made with the initial tension curves. The work hardening for all the curves during the first 1% deformation is very high and decreases rapidly. It then settles to fairly constant levels but in the case of the compression first curves this work hardening is twice as great (5.3 GPa compare to 2.4 GPa at 1% total deformation). Also, these curves start to yield at much lower stresses. In fact, the roundness of the curves is such that the measurement of the forward modulus and offset stress at  $10^{-4}$  plastic strain would show a significant inaccuracy and therefore was not done.

Some specimens of the unreinforced and composite materials were thermally cycled 5 times between R.T. and  $-196^{\circ}\text{C}$  in order to measure the effect of the difference of thermal expansion between the phases on the flow characteristics. All those specimens show an increase in their yield and subsequent flow stress relative to non-thermally cycled specimens. This is true for tests performed in tension and in compression (see figure 4.12 and 4.13). It also appears

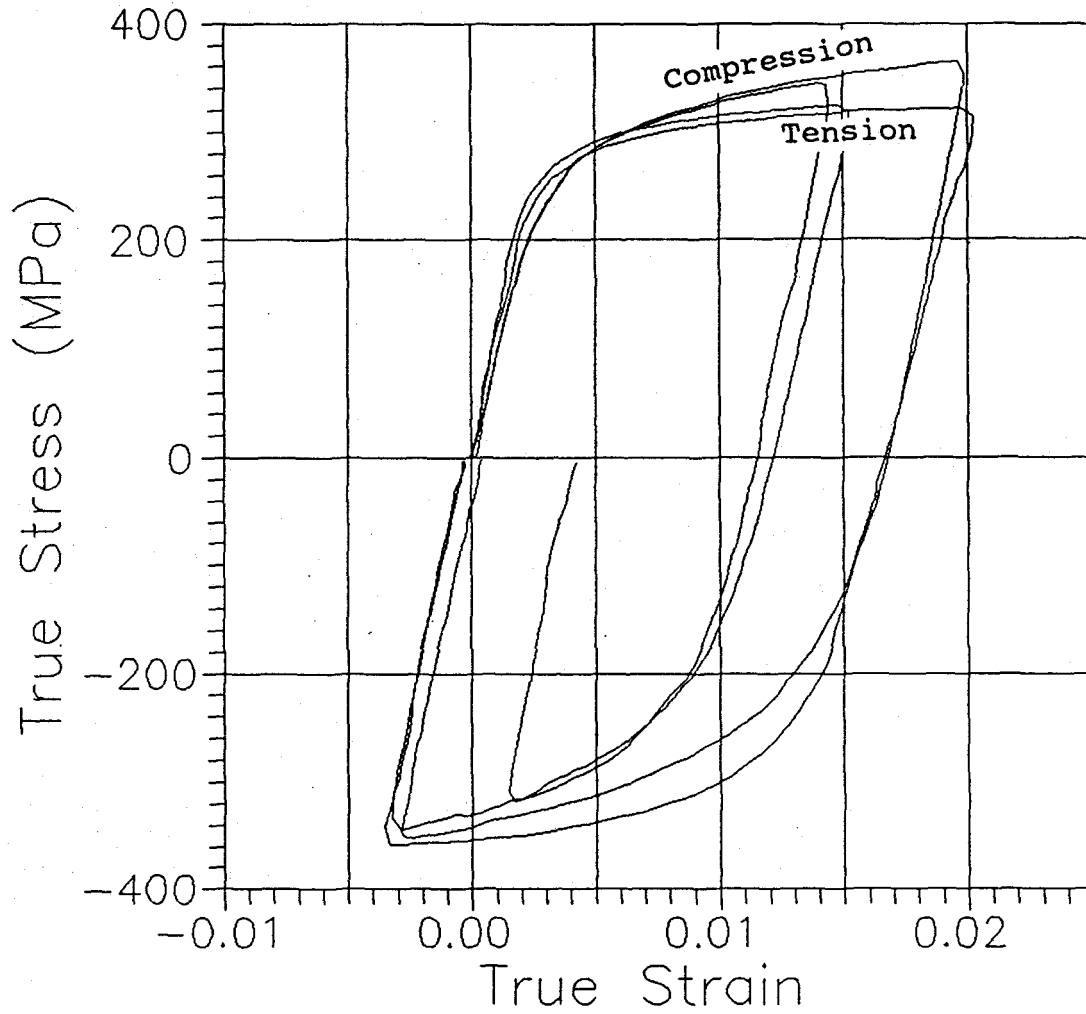


Figure 4.11 Hysteresis loop for the particulate composite for two specimens tested in compression-tension and two specimens tested in tension-compression. The compression first curves were reflected to begin in the first quadrant.

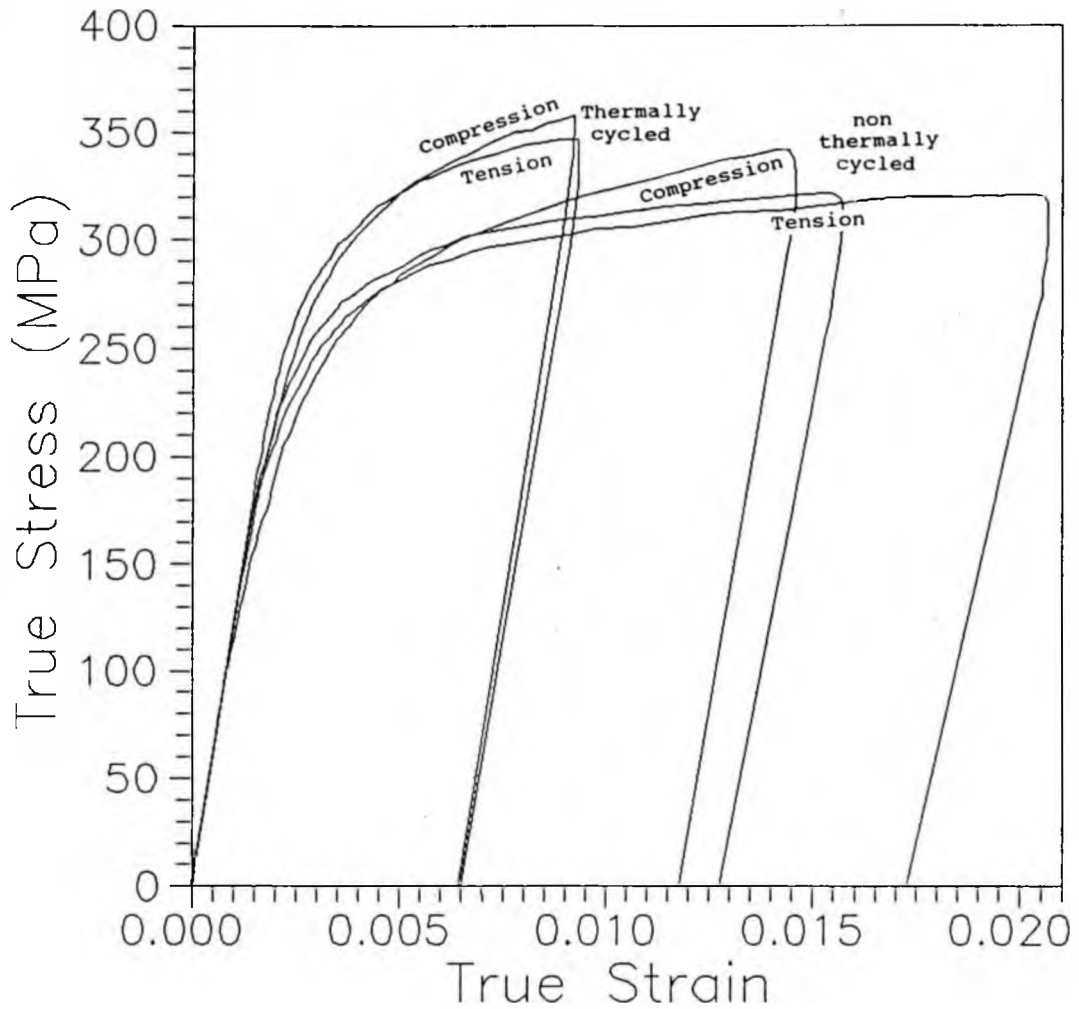


Figure 4.12 Stress strain curves of thermally cycled particulate composite material with non thermally cycled specimens.

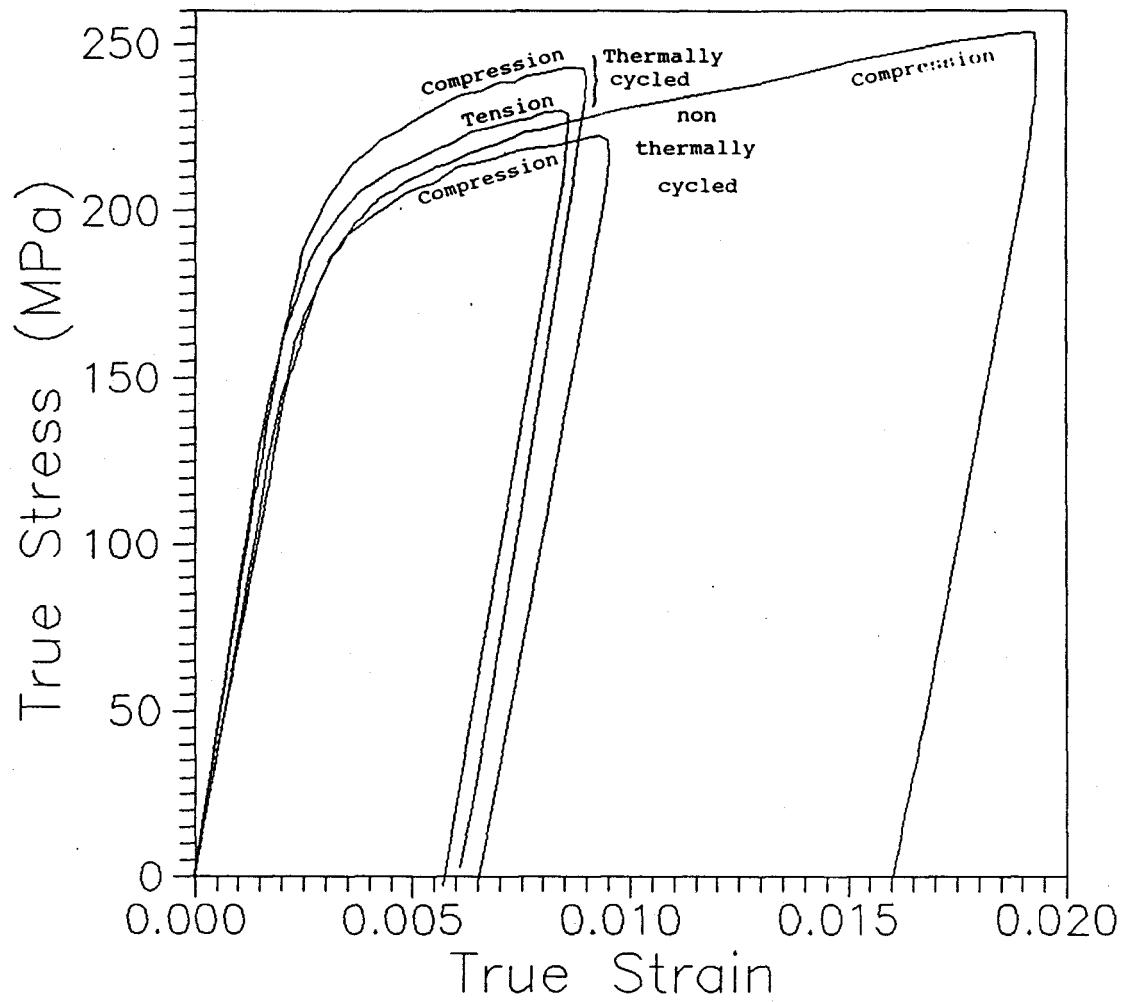


Figure 4.13 Stress strain curves of thermally cycled unreinforced material with non thermally cycled specimens.

that the work hardening for all thermally cycled specimens is similar to that obtained from non thermally cycled tests.

#### 4.3 Dimensional Instability:

The dimensional instability of the specimens compressed at  $-50^{\circ}\text{C}$  for both the particulate composite and unreinforced materials are shown in figures 4.16 and 4.17 respectively. The magnitude of the dimensional change for both materials is dependent on the subsequent heating temperature. The instability, or relaxation strain, is twice as great when heating at  $250^{\circ}\text{C}$  compared to  $155^{\circ}\text{C}$  ( $2 \times 10^{-3}$  compared to  $1.1 \times 10^{-3}$  for the composite material and  $1.5 \times 10^{-3}$  compared to  $0.8 \times 10^{-3}$  for the unreinforced). Other tests performed in liquid nitrogen gave similar results, showing that a decrease in the temperature below  $-50^{\circ}\text{C}$  does not affect the following dimensional change.

To verify the heating temperature range for which dimensional instability occurs, some specimens were compressed at  $-50^{\circ}\text{C}$  and then held at R.T. for a 24 hours period. No dimensional instability was observed. The effect of the level of deformation was further investigated by heating at  $250^{\circ}\text{C}$  some undeformed specimens. Again no dimensional instability was observed.

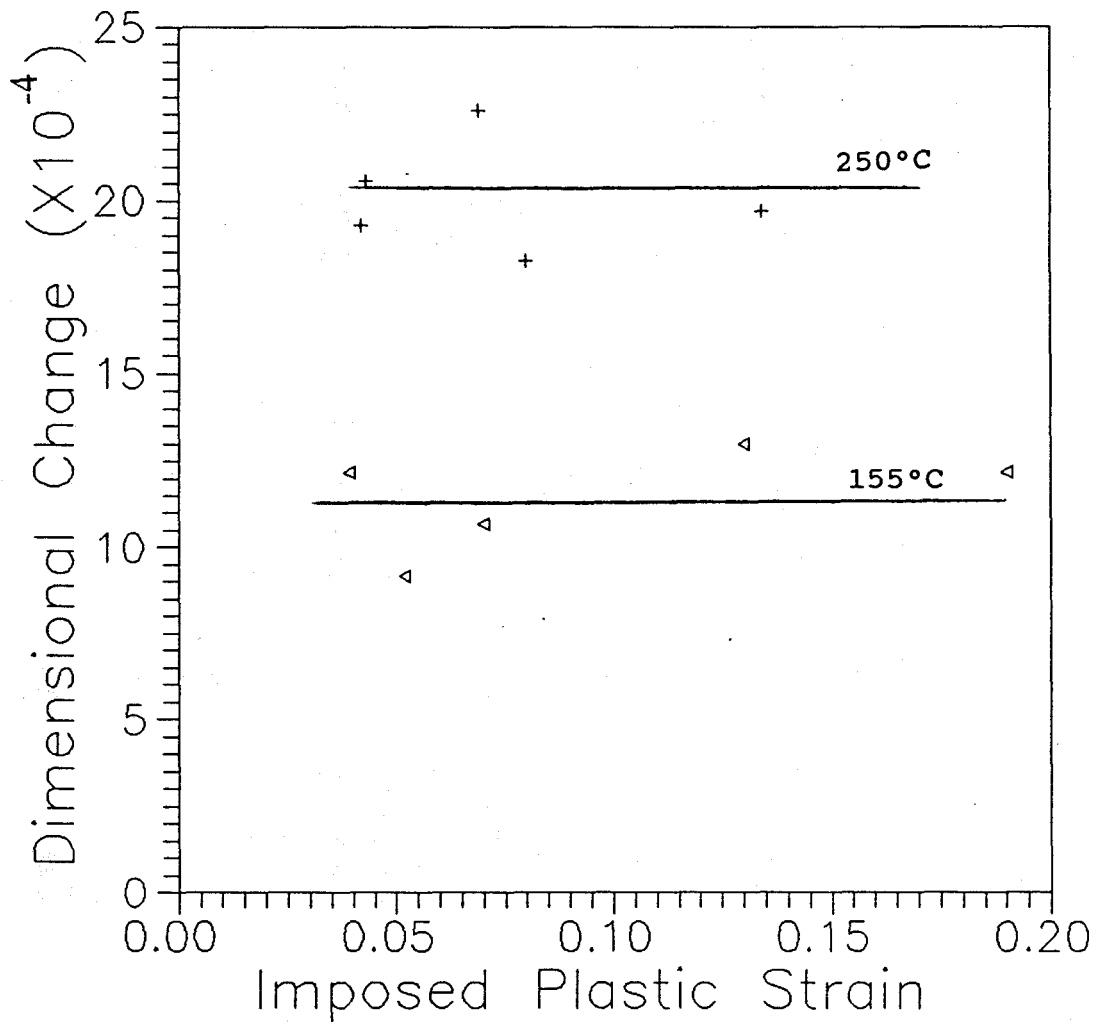


Figure 4.14 Dimensional instability results for the particulate composite material.

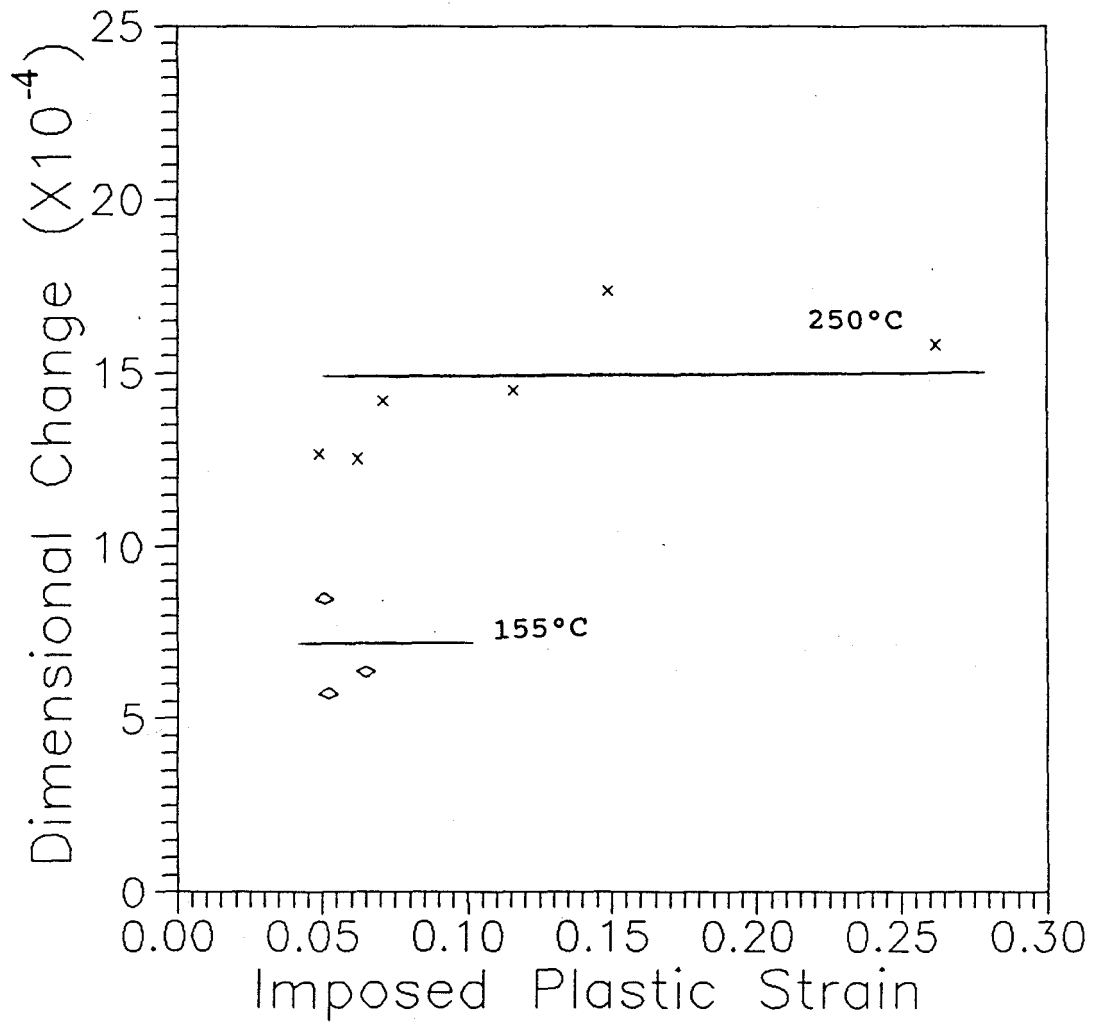


Figure 4.15 Dimensional instability results for the unreinforced material.

#### 4.4 Mechanical Properties of the Copper Tungsten Composite:

The basic mechanical properties of the Cu/W composite were extracted from the stress strain curves in figures 4.16 to 4.19 (table 4.5). These curves can be seen as being the superposition of the flow curve of the tungsten fibres and the copper matrix as in figure 2.2 in the literature review. The moduli  $E_I$  and  $E_{II}$  are for the linear portions of the curves during which the matrix and the fibres deform elastically ( $E_I$ ) and during which the matrix deforms plastically and the fibres elastically ( $E_{II}$ ).

This second modulus is relatively constant for each specimen with an average of 40 GPa. The first modulus shows more variation as expected since the matrix consists of very large grains. The yield  $Y_I$  of the composite represent the transition of the matrix from the elastic to plastic regime and is, as for the modulus  $E_I$ , strongly dependant on the orientation of the grains. The tungsten fibres could be heard breaking at a constant rate in the second stage of deformation of the composite. An audio recording of some of the tests allowed the rate to be evaluated to 2 to 6 fracture events per second. The specimens contained approximately 100 fibres. At such a rate and since the period during which the fibres were breaking was roughly 60 seconds, it is clear that some fibres

fractured more than once. Due to the large number of fibres in the specimens, the failure of a few fibres did not affect the stress strain curve. However, after a sufficient number of them broke, a sudden failure of a large number of the fibres occurs which makes the recording of the stress strain curve meaningless.

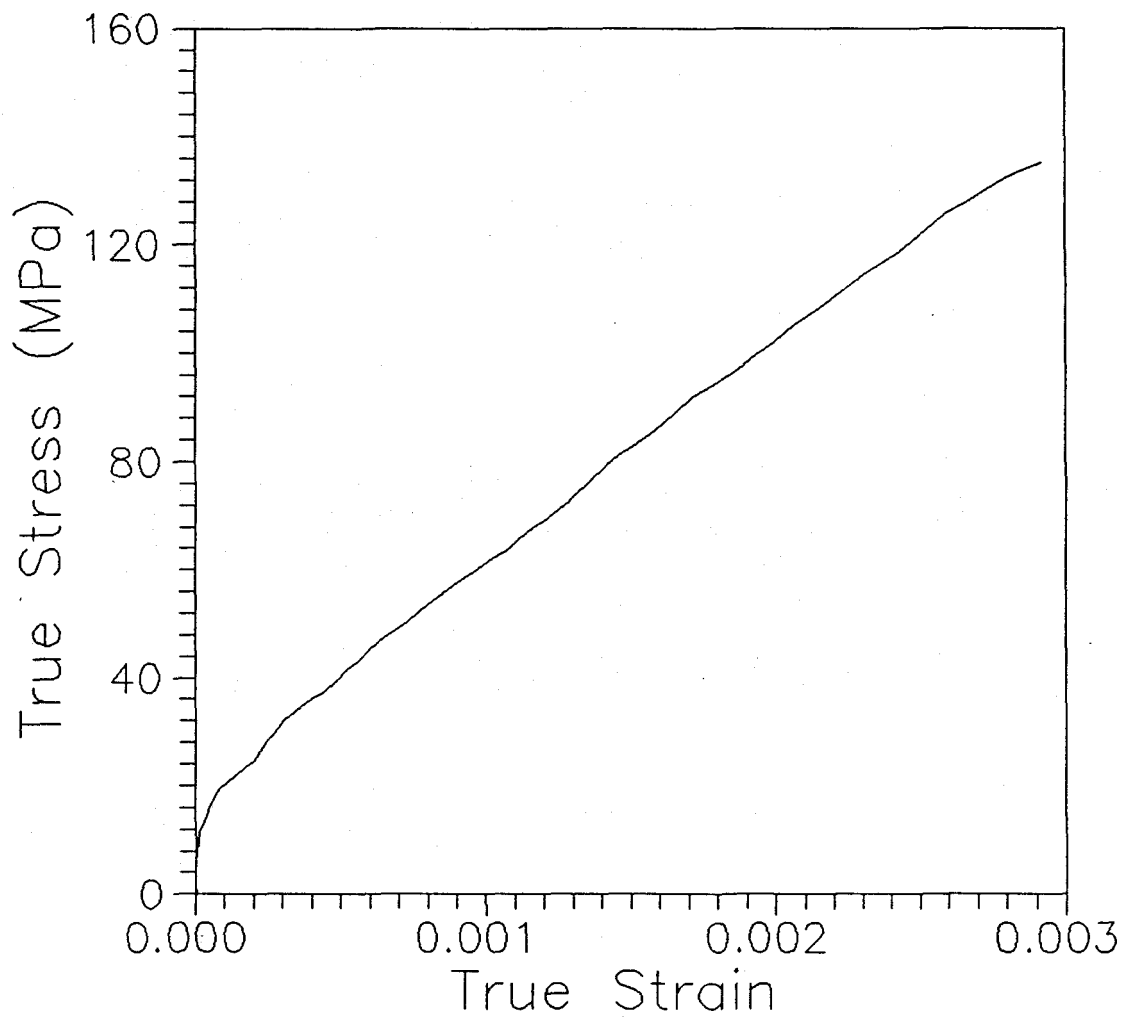


Figure 4.16 Stress strain curve of the Cu/W composite specimen #1.

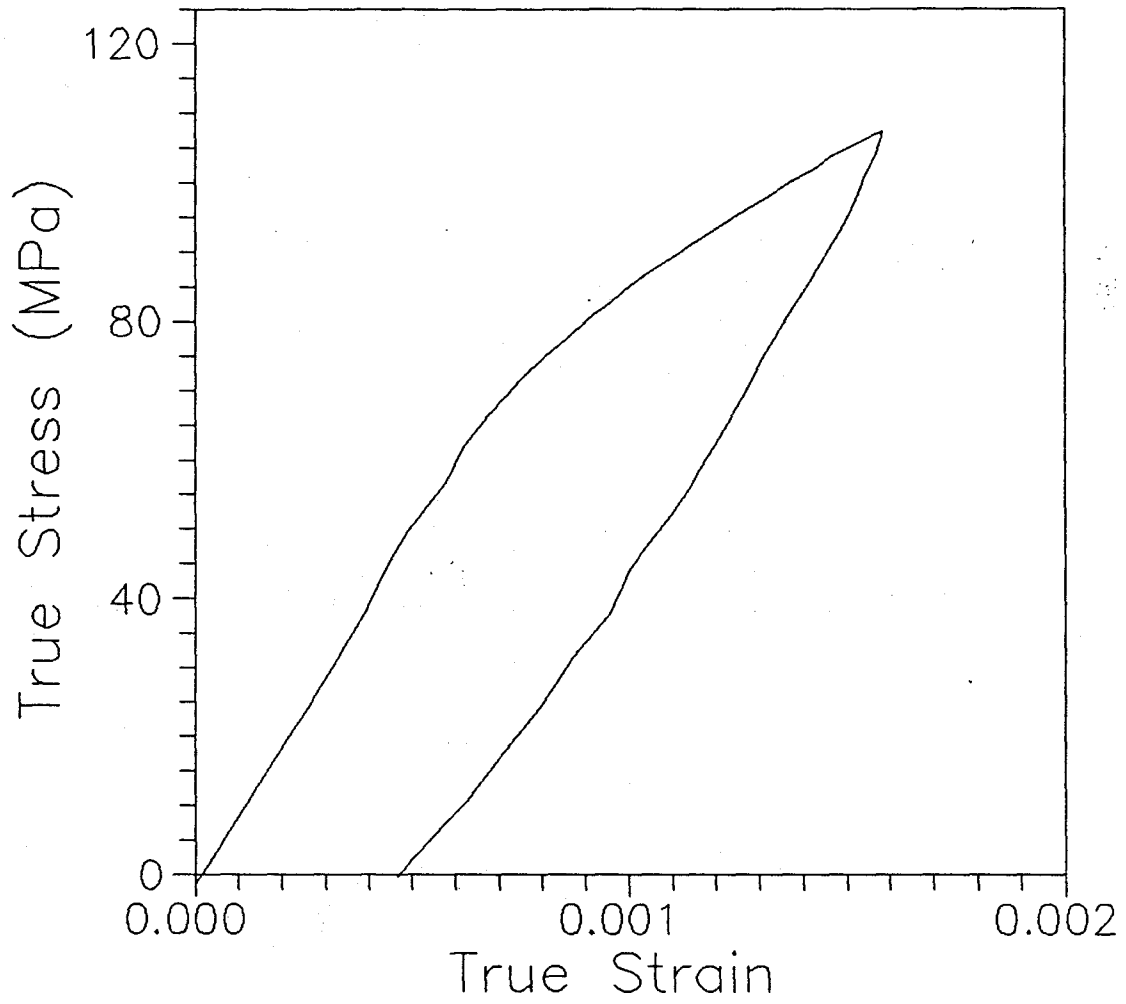


Figure 4.17 Stress strain curve of the Cu/W composite specimen #2.

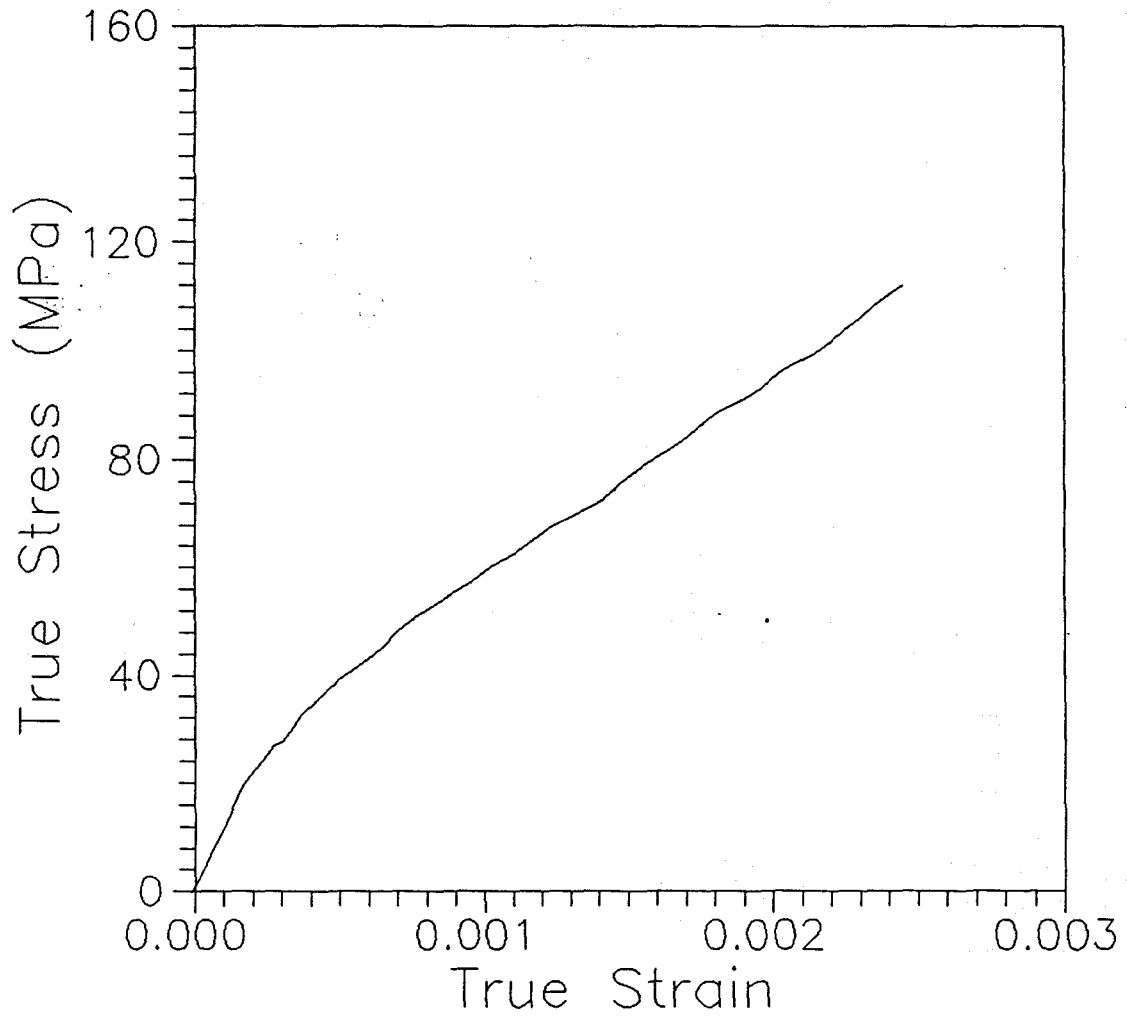


Figure 4.18 Stress strain curve of the Cu/W composite specimen #4.

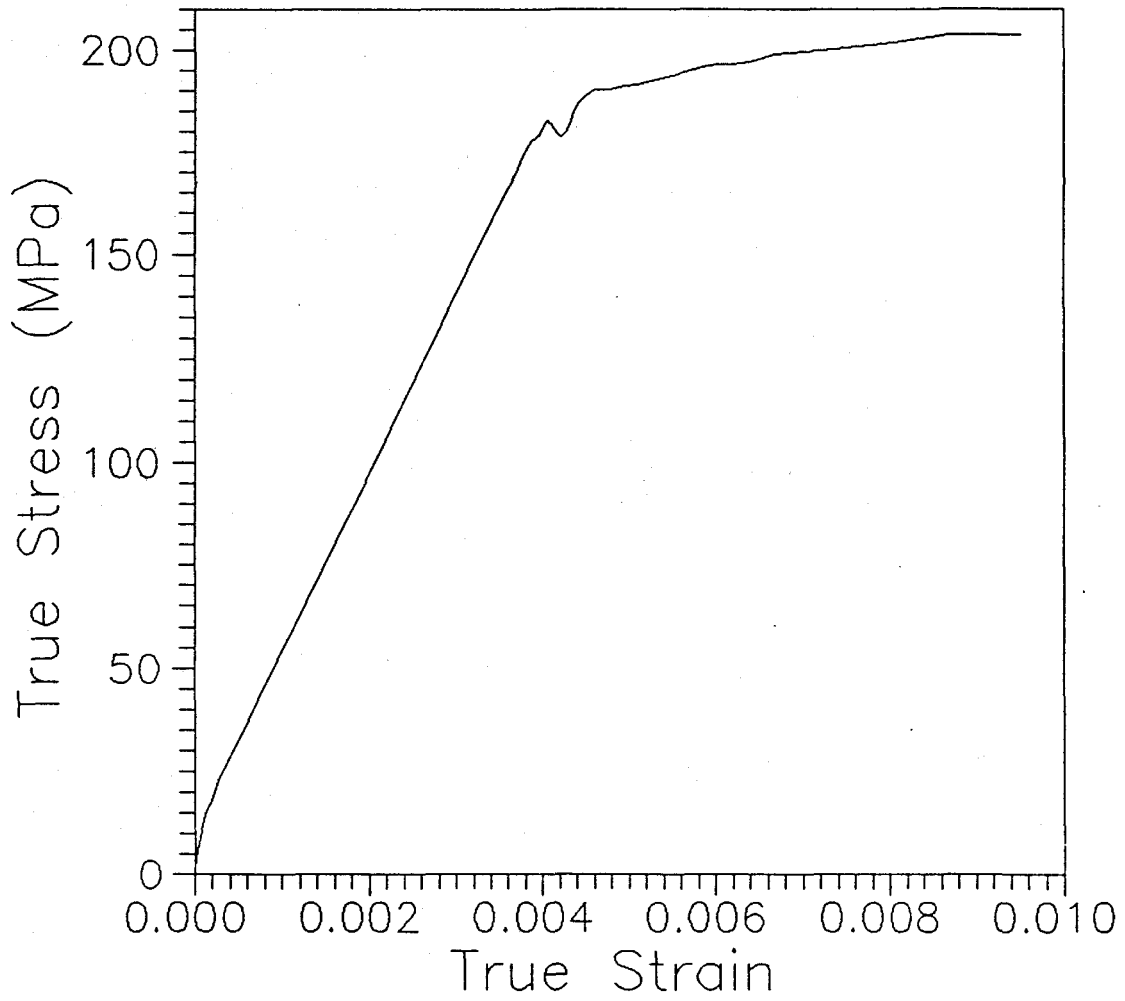


Figure 4.19 Stress strain curve of the Cu/W composite specimen #6.

	$E_I$ GPa	$E_{II}$ GPa	$Y_I$ MPa	$\epsilon_1$	$Y_2$ MPa	$\epsilon_2$
1	--	40	16	--	138	0.0029
2	109	40	64	0.0006	--	--
4	128	35	23	0.0002	122	0.0029
6	140	44	20	0.0011	190	0.004

Table 4.5 Results from the copper tungsten composite tests.

## **CHAPTER 5**

### **DISCUSSION**

The objective of this work was to define the effect of the addition of a particulate reinforcing phase on the mechanical behaviour of a metal matrix. The results from the copper reinforced with continuous fibres of tungsten experiments are analyzed first and are subsequently used in the following sections as a means of comparison with the particulate reinforced composite. The particulate composite and the unreinforced matrix are then analyzed first in terms of their monotonic loading behaviour and second in terms of the internal stresses development and saturation during the same deformation period. The results obtained from the thermally cycled specimens are then analyzed and compared with Arsenault and Shi's model and finally the dimensional instability results reported in chapter 4 are discussed in terms of the saturation level of internal stresses and from the viewpoint of a creep process.

#### **5.1 Model System Based on Copper with Continuous Tungsten Fibres:**

The analysis of the results obtained with samples of

copper reinforced with continuous tungsten fibres aligned along the loading axis can be considered by using the rule of mixtures. Assuming that the distribution of the fibres in the cross-section is uniform, the initial loading of the composite will make both phases deform elastically and equally to a strain  $\epsilon$  of the composite. All strains being equal, we can use the rule of mixtures to calculate the elastic modulus  $E_I$  of the composite

$$E_I = E_f \cdot V_f + E_m \cdot V_m \quad (5.1)$$

where m stands for matrix and f fibres. From the measurements of the elastic modulus of the composite  $E_I$  presented in table 4.5 and using a modulus of 350 GPa for the W (which is regarded in the literature as a minimum value), the results indicate that the modulus  $E_m$  of the matrix range from 82 to 116 GPa (see table 5.1). Since the matrix in this composite consists of a few large grains it is difficult to assess a precise theoretical value for its modulus. A lower bound value however is the modulus of a single crystal of Cu in [100] which is 70 GPa. The upper bound value using the same approximation is 185 GPa on [111]. Polycrystalline Cu has a modulus of 130 GPa (A.Kelly and H.Lilholt, 1969). The crystallographic orientation of specimen #2 in table 4.5 was measured after testing from a Laue pattern. The [111] direction was found to be 66° away from the loading axis

Specimen	Em (GPa)	$d\sigma/d\epsilon$ (GPa)
#1	--	5.5
#2	79	5.5
#4	100	0
#6	113	10
Cu [111]	185 <sup>1</sup>	--
Cu [100]	70 <sup>1</sup>	--
Cu polycrystal	130 <sup>2</sup>	2.6 <sup>3</sup>

Table 5.1 Calculated elastic modulus and work hardening rate of the copper matrix in copper tungsten composites. The elastic modulus of tungsten is assumed to be 350 GPa.

1: From E.Schmid and W.Boas, 1950

2: From A.Kelly and N.H.Macmillan, 1986

3: From A.Kelly and H.Lilholt, 1969. Average grain size of 30  $\mu\text{m}$

direction. The modulus of the matrix in this direction for specimen #2 was thus 79 GPa. The results obtained for  $E_m$  using the rule of mixtures of equation 5.1 are therefore consistent with the model.

The transition to plastic deformation of the matrix occurs very rapidly. After this transition the slope of the stress strain curve of the composite can be described at a given level of strain  $\epsilon$  in the matrix as

$$E_{II} = E_f \cdot V_f + V_m \cdot (d\sigma/d\epsilon)_{m,\epsilon} \quad (5.2)$$

where  $(d\sigma/d\epsilon)_{m,\epsilon}$  is the work hardening rate of the matrix at the plastic strain  $\epsilon$ . The tungsten fibres could be heard breaking during this second stage of deformation of the composite. However we found that this slope  $E_{II}$  was constant, indicating that the failure of the fibres did not reduce their load bearing effectiveness. The original aspect ratio  $l/d$  of the fibres was approximately 500 and it was found in specimen #4 and #6 that only 5 to 10% of these fibres broke during testing. The fractured fibres length was mainly in the range of 1 to 15 mm thus giving aspect ratios  $l/d$  from 10 to 150. The critical aspect ratio in metallic matrices is usually in the range of 40 to 80 (M.R.Piggott,1980). The remaining original fibres were thus sufficiently numerous and of large

enough aspect ratio for the composite to be unaffected by the failure of a small volume fraction of fibres during the second stage of deformation.

From the results of the slope of the second stage of deformation in the composite presented in chapter 4 (table 4.5) we can calculate the work hardening of the matrix and its relative contribution to the stress strain curves obtained for the composite. If we here again use a  $W$  modulus of 350 GPa we find the work hardening of the matrix to be between zero and 10 GPa. The contribution of the matrix is therefore minimal on the second stage deformation and represents a maximum of 20% of the slope  $E_{II}$ . A more realistic value for the modulus of  $W$  is 380 to 400 GPa, which would bring down the maximum contribution of the matrix to 10% of  $E_{II}$  according to the experimental results of this study.

We can therefore approximate the second stage deformation of this simple composite system to be

$$E_{II} = E_f \cdot V_f \quad (5.3)$$

as long as the aspect ratio of the fibres is greater than the critical aspect ratio. Equation 5.3 is in agreement with the results of Piggott (1980).

We will discuss in the next section whether this behaviour can be found in composite material with discontinuous reinforcements such as SiC particles.

## **5.2 Monotonic Loading of the SiCp Composite and Unreinforced Materials:**

A discontinuous reinforcing phase such as SiC particles in a soft matrix makes the analysis of the role of that phase on the overall composite mechanical properties very complex. We can take a macroscopic approach to the problem as we did for the Cu/W composite and evaluate the load carrying effect of the SiC particles on the stress strain relationship of the composite. If we make the assumption that the volume fraction of SiC is the one of continuous SiC fibres, we can calculate the maximum theoretical elastic modulus that the composite of this study could have. The particles in the composite are not oriented preferentially in one direction. The extreme situations arise when these fibres are assumed to be all oriented parallel or perpendicular to the loading axis of the composite specimens. These two cases can be used as assumptions that will give an upper and lower bound estimate of the effect of SiC on the elastic modulus of the composite.

If we assume that these SiC fibres are all oriented in the loading axis of the composite specimens, we can use

equation 5.1 since both the matrix and the fibres are strained equally. With an elastic modulus for SiC equal to 400 GPa (A.Kelly and N.H.MacMillan, 1986) and with the matrix elastic modulus of 73 GPa that was experimentally found (table 4.3), we get for a volume fraction of 20% SiC a composite modulus of 138 GPa. This result is 25 GPa higher than the average results obtained for the composite (114 GPa). The rule of mixtures given by equation 5.1 thus gives an overestimated value for the modulus of the composite  $E_1$ .

If the SiC fibres are assumed to be perpendicular to the loading axis, the imposed strain on the composite is different from the strain of the SiC and from the strain of the matrix. Both phases however are subjected to the same applied stress the composite is subjected to which allows to estimate the modulus of the composite as being (M.R.Piggott, 1980)

$$1/E_1 = V_f/E_f + V_m/E_m \quad (5.4)$$

and gives a composite modulus of 87 GPa.

The experiments showed an average modulus of 114 GPa, which thus lies within the upper bound (138 GPa) and lower bound (87 GPa). Predicting more precisely the modulus of the composite is clearly difficult since the reinforcing phase is

discontinuous.

Repeating the same calculation for the unreinforced material with a modulus for the Si precipitates of 130 GPa (A.Kelly and N.H.Macmillan, 1986), 69 GPa for the modulus of pure Al and a volume fraction of 5% gives a theoretical maximum elastic modulus for the unreinforced material of 72 GPa according to equation 5.1. Considering the accuracy of the measurements and the assumptions involved, this maximum value of the unreinforced modulus, the unreinforced modulus obtained experimentally and the modulus of pure Al are so close that we cannot draw any conclusion as to whether or not the Si precipitates play a significant role in the modulus of the unreinforced material.

As opposed to the Cu/W results the transition from elastic to plastic deformation of the matrix in the Al/SiC composite system occurs over a range of strains. The slope of the stress strain curves decreases rapidly after the yield of the material. The very high rate of work hardening in this transition from elastic to plastic deformation is undoubtedly related to the presence of the SiC particles and the heterogeneous stress state in the microstructure.

The experimental results obtained give the slope of the stress strain curve at 1% plastic deformation equal to

approximately 1.5 GPa (figure 4.3). We can therefore see that in the second stage of deformation (reinforcement elastic, matrix fully plastic) of the composite material the SiC particles have no effect on the rate of the flow curve and that this rate is essentially the one of the work hardening of the matrix. This is in contradiction with stage I of the deformation where the particles were playing a major role on the modulus of the composite. A better understanding of the effect of the SiC particles during the deformation of the composite can arise from the observations made on the evolution of the internal stresses as the composite is deformed.

### **5.3 Reverse Loading of the SiC<sub>2</sub> Composite and Unreinforced Materials:**

As mentioned in the literature review the forward straining of composite materials allows the development of internal stresses which are related to the degree of the plastic deformation. The reverse loading experiments done in this study allow an evaluation of the extent and evolution of the internal stresses and help in interpreting the effect of the SiC particles and Si precipitates on the mechanical properties of composites.

The evolution of the backstress with increasing imposed deformation as shown in figure 4.7 to 4.10 can be represented by two different steps. The first one concerns the initial linear increase of the backstress during which no relaxation mechanisms take place. The materials see the level of internal stresses increase to the limit of which the particles (precipitates) can sustain. The second step begins when the increase in backstress becomes non linear, that is the material can no longer support the increase of internal stresses. Relaxation of these internal stresses then occurs and is an indication that the material reaches a level of saturation of internal stresses due to the intervention of an additional process such as the fracture of the reinforcing phase.

The first step in the evolution of the backstress can be viewed from two different scales. On a microscopic scale it is possible to attempt a modelling of the process using such parameters as the shape of the particles or precipitates and the intrinsic strength difference between these phases and the matrix. Or from a macroscopic view point modelling can be done in terms of simply the different volume fraction of the phases assuming they are continuous.

The backstress in single crystals can be evaluated from the permanent softening as described in the literature

review. Complications arise when a material contains large volume fraction of discontinuous reinforcement as in the particulate material. The absence of permanent softening observed has brought the utilization of the backstress definition of equation 2.7. The backstress measured is therefore related to the assumption that the unloading of the material, after the forward deformation, does not create a change in the internal stress structure. That is the internal stresses remain present (or are not modified) during the unloading.

The estimation of the backstress in unrelaxed materials based on a microscopic approach can be done based on Eshelby's calculations for dispersion hardened materials. The size of the particles in these materials range from 5 to 500 nm and the volume fraction from 0.01 to 1 percent. The microstructure in the composite material of this study has much coarser particles and larger volume fraction and therefore the fundamental basis of these estimations might not apply to this composite system. We can apply Brown and Clarke's relation (1975) (as suggested by these authors for materials containing a volume fraction and an average particle size of the order of those relevant to the current composite material)

$$\sigma_B = 2\gamma D\mu f\epsilon_p \quad (5.4)$$

where  $\gamma$  is a shape factor , D a strength differential factor,  $\mu$  the shear modulus of the matrix and f the volume fraction of the particles (or precipitates). Then following Lilholt (1976) we get a ratio of

$$d\sigma_B/d\epsilon_p = 6\gamma D\mu f / (1 - fD) = 42 \text{ GPa} \quad (5.5)$$

This tensile backstress rate is based on a Schmid factor for fcc polycrystal of 3 (G.I.Taylor,1938),  $D=1.8$ ,  $\gamma=0.53$ ,  $\mu=26$  GPa. This ratio should be further increased due to the effect of the 5% volume fraction of silicon precipitates. This is therefore comparable to the 50 GPa obtained experimentally (figure 4.7) using the  $10^{-4}$  offset strain. The reasons that could explain the lower theoretical value are that the shape factor  $\gamma$  used in the calculation is the one for spheres, which may not be representative of the actual shape of the SiC particles, and the very large total volume fraction of reinforcing phases, 25%, which makes it possible for the stress field surrounding the particles to interact with neighbouring particles' stress field. However more important is the assumption made that no backstress are present initially in the materials. The effect of such internal stresses is that the measured slope of 50 GPa should be in fact less and possibly closer to the expected predictions from this model.

It is likely that some degree of internal stresses are initially present in the materials (both the composite and the unreinforced). This is indicated to a certain extent by the different yield stresses obtained when the first portion of the tests are done in tension or in compression. In the case of the composite material an average difference of yield stress between tension and compression of 35 MPa is observed when the yield stress is measured using an offset strain of  $10^{-3}$ . For the unreinforced material this difference is 20 MPa for both  $10^{-4}$  and  $10^{-3}$  offset strains (see table 4.3). If we therefore assume that an initial internal stress of 35 MPa is present in the composite prior to testing, then the backstress results shown in figure 4.7 could be set to begin at 35 MPa instead of zero. The result is a slope of 32 GPa which is slightly less than the expected result of 42 GPa (equation 5.5). We can therefore see that the assumption made that the backstress is zero initially gives an upper bound value of  $d\sigma_B/d\epsilon_p$ , and when an initial elastic stress is assumed to be present a lower bound value is obtained.

A model based on a microscopic or dislocation approach such as the one previously defined therefore does seem to be applicable to discontinuously reinforced materials with reinforcing phase of above the micron scale. A macroscopic model of the deformation of a composite could consist of

assuming that the reinforcing phase is in the form of continuous fibres uniformly distributed along the loading axis (as in section 5.2). Taking equation 5.2 used to evaluate  $E_{II}$  gives

$$\sigma_{II} = E_{II}\epsilon_p \quad (5.6)$$

Since we found in the composite model that the contribution of the matrix to the slope  $E_{II}$  is minimal, from equation 5.5 and 5.6 we get

$$\sigma_{II} = (V_f E_f) \epsilon_p \quad (5.7)$$

We now have to define the internal stress arising from the presence of 2 distinct phases put together. Both phases are subjected to the same deformation  $\epsilon_p$  but each supports a different stress  $\sigma$ . If we make the approximation that during the loading of this composite model in the second stage deformation a residual stress is developed equal to the difference in stresses between the 2 phases, we find (assuming no stress relaxation)

$$\sigma_B = (\sigma_f - \sigma_m) \quad (5,8)$$

or since the contribution of the matrix is minimal

$$\sigma_B = \sigma_f \quad (5,9)$$

and from 5.7 and by replacing  $\epsilon_p$  by the unrelaxed strain  $\epsilon_p^*$  contributing to the development of residual stress

$$\sigma_B = (V_f E_f) \epsilon_p^* \quad (5,10)$$

$\epsilon_p^*$  can be defined with respect to  $\epsilon_p$  as being a fraction of the latter. The unrelaxed strain is large at low strain levels by comparison with the total plastic strain. This ratio  $\epsilon_p^*/\epsilon_p$  however decreases as the plastic strain increases beyond a certain level of  $\epsilon_p$  when the unrelaxed strain does no longer increase substantially. This ratio has not been determined experimentally but can be set as  $\frac{1}{2}$  for the sake of simplicity for plastic strains less than 0.5%. This is the plastic strain at which a departure from linearity in the backstress versus plastic strain plots was observed (figure 4.7 to 4.10).

Applying equation 5.10 to the Al/SiC composite material gives a ratio

$$\sigma_B/\epsilon_p^* = 40 \text{ GPa}$$

This result does correspond to the range of rates of increase of the backstress of 32 to 50 GPa found when an internal stress of 35 MPa is assumed to be initially present in the material prior to testing and when no such assumption is made. The applicability of this model therefore supports the concept that the SiC particles act like fibres in the composite up to a certain degree of plastic deformation if we

take into consideration some level of initial internal stresses. The elastic modulus of the composite  $E_T$  (see section 5.2) and the initial rate of increase of  $\sigma_B$  can therefore be modeled on a macroscopic basis assuming the SiC phase to be in the shape of fibres. Both the predictions from the microscopic and macroscopic models are plotted in figure 5.1 for different volume fraction of SiC. The experimental data from this work are also on the figure and are in accordance with the models.

The second step in the evolution of the backstress as the deformation is increased begins in the composite material after about 0.4% plastic strain. The development of backstresses decreases and saturates (0.9% plastic strain). The magnitude of the backstress becomes constant, the development and relaxation rates becoming equal. This behaviour in fact coincides with the rapid decrease in the slope of the monotonic curve as mentioned in section 5.2. At approximately 0,7% plastic deformation the slope of the monotonic curve has already reached about 3.5 GPa, slightly above the work hardening of the matrix, and the backstress in the composite is approaching its maximum value of 200 GPa.

Both phenomenon therefore seem to indicate a change in the effect of the SiC particles in the deformation of the composite. This can be related to the magnitude of internal

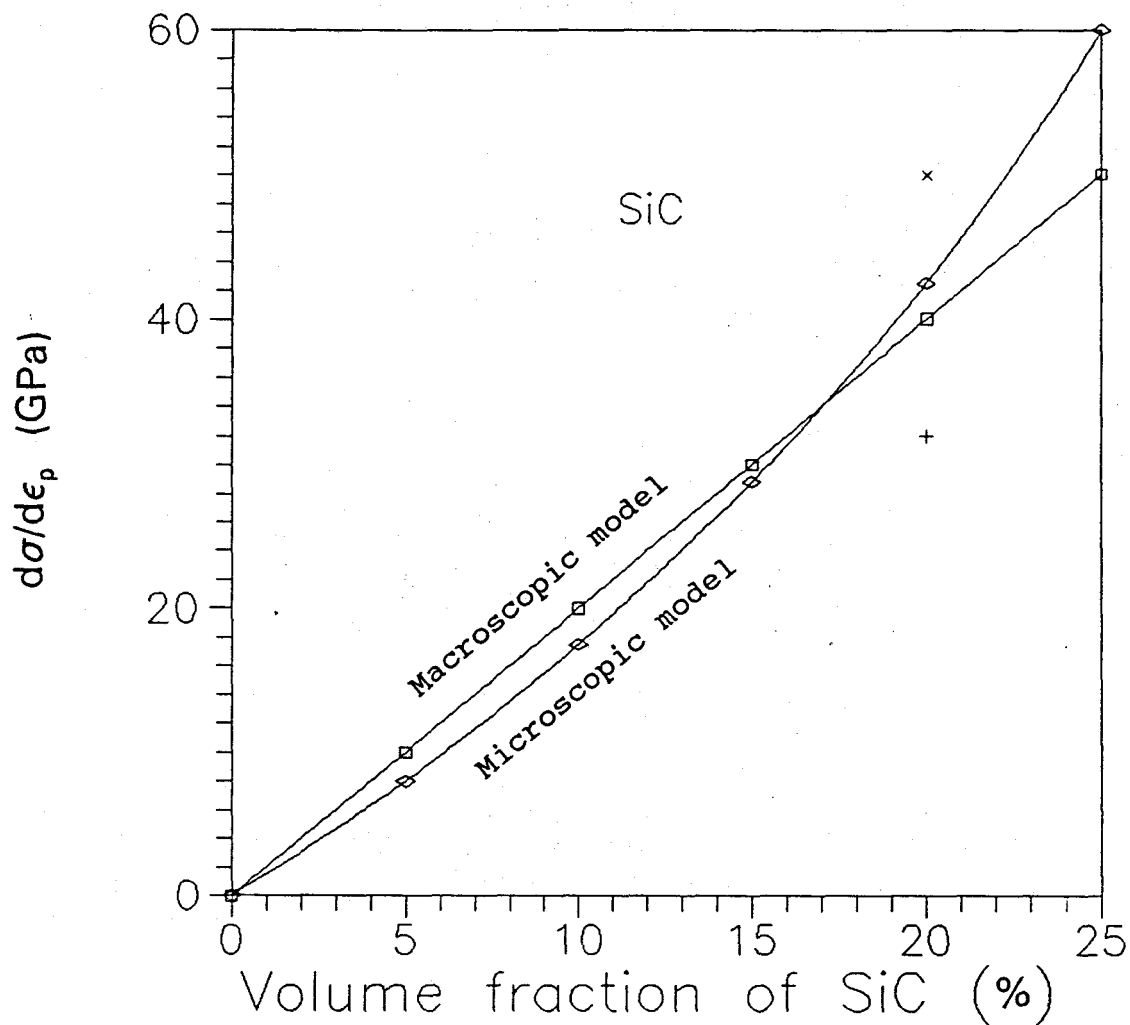


Figure 5.1 Rate of increase of the unrelaxed backstress  $\sigma_B$  for different volume fraction of SiC using a) a microscopic model (equation 5.5) and b) a macroscopic model (equation 5.10). The experimental results are plotted assuming no initial internal stresses (X) and an initial internal stresses of 35 GPa (+).

stresses in the material. The relaxation of the elastic strain in the composite occurs when the level of backstress in the matrix, divided by the volume fraction of SiC, reaches the strength of these particles. The mean backstress in the matrix is equal to the elastic stress in the particles. The 2 phases however are not present in equal volume fraction and therefore the stress carried by the particles has to be weighed up by its volume fraction (20%). The stress born by the SiC<sub>p</sub> is thus around  $200 \text{ MPa}/0.20 = 1 \text{ GPa}$ . Since the SiC particles bear essentially the majority of the backstress due to their high strength, the deformation or fracture of them implies that the backstress cannot be further increased and carried by the composite material. As a result of this the backstress reached a maximum as shown in the figures 4.7 and 4.8.

The SiC particles can therefore be viewed in the composite material as "grains" of a second phase with higher stiffness and strength (see figure 2.6a in the literature review). The SiC<sub>p</sub> size is indeed approximately the same as the matrix grains size. When the surrounding matrix grains begin to deform, stresses are built up on the second phase "grains". At the failure of these "grains" (which does not occur simultaneously everywhere in the material since the stress state in the microstructure is heterogeneous), stresses are released and the surrounding matrix grains can more easily

flow. The SiC does no longer play a significant role in the flow characteristic of the composite which in fact becomes the one of the matrix grains.

The unreinforced material with its 1 to 2 micron size Si precipitates and its 5% volume fraction cannot be described as a dispersion hardened material nor a composite on the macroscopic scale. Using the dispersion hardened model and Lilholt equation 5.5 gives an expected rate of increase of the backstress of approximately 5.8 GPa ( $D=1.32$ ). From the macroscopic model leading to the equation 5.10 we get a backstress of about 3.3 GPa. Both models fall short of the 17 GPa obtained experimentally assuming no initial internal stresses. The difference in the yield stress between tests done in tension and in compression is 20 MPa. The minimum value for the rate of increase of the backstress is therefore, assuming an initial backstress of 20 MPa, about 10 GPa. Other mechanisms therefore must give rise to the development of the backstress than the sole presence of the Si precipitates. The presence of an internal stress gradient in the material prior to testing for example might be worth considering (Sowerby et al., 1979). It appears however that the Si precipitates in the unreinforced material of this study do not behave as the SiC particles in the composite material. In part due to their small size (an order of magnitude smaller than the SiC<sub>p</sub> and

the matrix grain size) and low volume fraction. The maximum backstress developed however does correspond to approximately the strength of the Si precipitates ( $130 \text{ MPa}/0.05 = 2.6 \text{ GPa}$ ). The relaxation of the elastic stress is thus related to the failure of the Si precipitates in the matrix. This is in agreement with recent work by Hunt et al. (1990) that showed that Si precipitates in aluminum begins to fail at a very early stage of plastic deformation (1% plastic).

The backstress results for both the composite and the unreinforced materials have shown a dependence on the testing temperature. Several mechanisms involved in the development and relaxation of the backstress in the Al matrix material are temperature related.

The strength of the reinforcing phase is a critical parameter in the magnitude of the backstress. The strengths however of the SiC and Si phases are not significantly affected by a decrease in temperature of  $70^\circ\text{C}$  from R.T. (G.Q.Weaver and B.A.Olsen,1973). The work hardening however of Al is strongly dependent on the testing temperature. The rate of the work hardening of >99.987% Al was observed (R.P.Carreker and W.R.Hibbard,1957) to be equal, at 1% total strain, to 0.73 GPa at R.T. and 1.03 GPa at  $-78^\circ\text{C}$  (average grain size diameter of 65  $\mu\text{m}$ ). This difference in work hardening rates becomes greater at 2% total strain (0.46 GPa

compared to 0.72 GPa). This means that the magnitude of the backstresses developed in pure Al is greater when the deformation of the material is done at  $-78^{\circ}\text{C}$  than at R.T. If the backstress results obtained on the composite material are normalized by the work hardening rate of pure Al at 1% total strain, the results at  $-50^{\circ}\text{C}$  (200 MPa) and R.T. (150 MPa) become  $194 \times 10^{-3}$  and  $204 \times 10^{-3}$  respectively. The difference still present between the two temperature should originate from the fact that the work hardening measured at  $-78^{\circ}\text{C}$  was used to normalize a  $-50^{\circ}\text{C}$  result. The work hardening of pure Al at  $-50^{\circ}\text{C}$  should be less than the one measured at  $-78^{\circ}\text{C}$  and therefore the normalized  $-50^{\circ}\text{C}$  result should be closer to the normalized R.T. result.

In the case of the unreinforced material the 130 MPa ( $-50^{\circ}\text{C}$ ) and the 95 MPa (R.T.) backstress, after normalization at 1% deformation, become  $126 \times 10^{-3}$  and  $130 \times 10^{-3}$  respectively.

The different backstress results obtained at the two testing temperatures for both materials appear to be due to the temperature dependence of the work hardening rate of the Al matrix. This dependence was also reflected in the slope of the monotonic curves of the composite and unreinforced materials. For these materials the slope at 1% deformation

increases by approximately 35% and 30 % respectively when tested at  $-50^{\circ}\text{C}$  compared to R.T.

#### 5.4 Thermally Cycled Specimens:

The effect of thermal cycling between  $25^{\circ}\text{C}$  and  $-196^{\circ}\text{C}$  the specimens made of both the unreinforced and the particulate composite materials is evident in figures 4.12 and 4.13. The increase in the flow stress, relative to not thermally cycled specimens, can be explained by the presence of a greater dislocation density which increases the yield stress of the materials. The mechanism at the origin of this increase of dislocation density is the difference in the coefficient of thermal expansion (CTE) between the aluminum and the particles and precipitates. The CTE for the aluminum is 6 times greater than that of the SiC (CTE Al =  $24 \times 10^{-6} \text{ K}^{-1}$  and CTE SiC =  $4 \times 10^{-6} \text{ K}^{-1}$ ) and 10 times that of Si (CTE Si =  $2.5 \times 10^{-6} \text{ K}^{-1}$ ). A decrease in temperature of about 221 K such as experienced by the composite and the unreinforced materials is sufficient for the interface between the SiC, or Si precipitates and Al to be strained plastically in tension, thus increasing the dislocation density in the Al matrix. The difference in CTE between Al and SiC ( $\Delta\alpha$ ) is  $20 \times 10^{-6} \text{ K}^{-1}$  and therefore

$$\epsilon = \Delta\alpha\Delta T \quad (5.11)$$

$$\epsilon = 20 \times 10^{-6} \times 221$$

$$\epsilon = 4.4 \times 10^{-3}$$

and for the Si precipitates  $\Delta\alpha$  is  $21.5 \times 10^{-6}$  so

$$\epsilon = 4.8 \times 10^{-3}$$

These values are well above the strains necessary to deform plastically these materials at R.T..

It is possible using the results to estimate the increase in dislocation density using a simple relation between the flow stress  $\sigma$  and the dislocation density  $\rho$

$$\sigma = \alpha G b \rho^{1/2} \quad (5.12)$$

where  $\alpha$  is a constant equal to 1.25 (N.Hansen,1977),  $G$  is the shear modulus of the matrix and  $b$  the Burger's vector. The initial dislocation density  $\rho_0$  in the materials is unknown and cannot be reliably determined by 5.12 since the materials in this study contain second phases which affect their flow stress. However the increase in dislocation density arising from thermal stresses has been evaluated based on 5.12 from the increase in flow stress for both materials, and for both tensile and compression tests at a plastic strain of 0,6% (table 5.2).

The increase in flow stress after the thermal cycling then allows an evaluation of the corresponding increase in

dislocation density, assuming a linear additivity of the stress components. These calculations were done and are also presented in table 5.2.

If we consider Arsenault and Shi's model of the increase in dislocation density due to the CTE as shown in equation 5.13

$$\rho_i = K\Delta\alpha\Delta TV_f/bt(1-V_f) \quad (5.13)$$

we can evaluate the extent of increase of the dislocation density and compare these predictions with the experimental results obtained using equation 5.12. This model assumes the dislocation density increase to arise solely from the punching of dislocations from the particles. However, the high volume fraction of particles combined with the large difference in the coefficients of thermal expansion can cause regions in the microstructure to be subjected to severe stresses during thermal cycling. Plastic deformation of these regions, and therefore an increase in dislocation density, might also be responsible for the increase in density. The geometric constant  $K$  range from 4, for platelet, to 12 for spheres and  $t$  is the average smallest side length of the particles. In the case of the spheroidal Si precipitates  $t$  is equal to the average diameter of the precipitates (1.5  $\mu\text{m}$ ) and for the SiC

		$\Delta\sigma$	$\Delta\rho$	$\rho_r^1$
Composite/uncycled /tension $\sigma_o = 310$ MPa	Composite/cycled /tension $\sigma = 340$ MPa	30	10.4 $\times 10^6$	13.2 $\times 10^6$
Composite/uncycled /compression $\sigma_o = 320$ MPa	Composite/cycled /compression $\sigma = 370$ MPa	50	29.2 $\times 10^6$	13.2 $\times 10^6$
Unreinf./uncycled /tension $\sigma_o = 215$ MPa <sup>2</sup>	Unreinf./cycled /tension $\sigma = 235$ MPa	20	4.6 $\times 10^6$	7 $\times 10^6$
Unreinf./uncycled /compression $\sigma_o = 222$ MPa	Unreinf./cycled /compression $\sigma = 250$ MPa	28	9.0 $\times 10^6$	7 $\times 10^6$

$$\rho = (\sigma/\alpha Gb)^2 \quad \Delta\rho = (\Delta\sigma/\alpha Gb)^2 \quad \rho_r = K\alpha\Delta TV_f/bt(1-V_f)$$

$$\alpha = 1.25 \quad b = 286 \times 10^{-9} \text{ mm} \quad G = 26\,000 \text{ MPa}$$

$$\text{CTE Al} = 24 \times 10^{-6} \text{ K}^{-1}$$

$$\text{CTE SiC} = 4 \times 10^{-6} \text{ K}^{-1}$$

$$\text{CTE Si} = 2.5 \times 10^{-6} \text{ K}^{-1}$$

$$\Delta T = 221 \text{ K} \quad V_f \text{ SiC} = 20\% \quad V_f \text{ Si} = 5\%$$

$$t \text{ SiC} = 0.005 \text{ mm} \quad t \text{ Si} = 0.0015 \text{ mm}$$

$$K \text{ SiC} = 8 \quad K \text{ Si} = 12$$

<sup>1</sup>: The dislocation density for the composite was evaluated as the sum of the dislocation density arising from the SiC and arising from the Si ( $6.2 \times 10^6 + 7 \times 10^6 = 13.2 \times 10^6$ )

<sup>2</sup>: Approximation

Table 5.2 Dislocation density results ( $\Delta\rho$ ) and theoretical ( $\rho_r$ ) in the thermally cycled specimens.  $\Delta\rho$  is the increase in dislocation density calculated from equation 5.12.  $\rho_r$  is the calculated dislocation density from Arsenault and Shi's model (equation 5.13).

particles  $t$  is equal to 6  $\mu\text{m}$  (average particle diameter=12  $\mu\text{m}$ , aspect ratio=2). Using for the Si precipitates a value  $K=12$ , for the  $\text{SiC}_p$ , the average value  $K=8$  and the other data listed in table 5.2, we obtain predicted densities in agreement with those obtained previously from the stress strain results. These predictions fall in between the range of results obtained using the tensile and compression tests.

We can further see using this model that the influence of the  $\text{SiC}_p$  and its CTE on the production of dislocations is equal to the effect of the Si precipitates. The proportion of dislocations arising from the presence of the  $\text{SiC}_p$  in the matrix represents 1/2 of the total production of dislocations during thermal cycling. The reason for this is that even if the Si precipitates represent only 1/5 of the volume fraction of the total "reinforcements", their diameter is 1/3 of that of the  $\text{SiC}_p$ . According to Arsenault and Shi's model the effectiveness of the Si precipitates to produce dislocations by thermal cycling is therefore as great as for the  $\text{SiC}_p$ . The size of the reinforcing phase is therefore an important factor in the increase of dislocation density by thermal cycling.

The experimental results show that the ratio of the average increase in dislocation density in the composite material relative to the unreinforced material is in the range

of 2 to 3. Assuming that the effect of the SiC particles and the Si precipitates on the production of dislocations can be added to give the increase in the composite material, this ratio should be 2 in theory. The experimental results are therefore in good agreement with the model and confirm the assumption that the dislocation density production from different sources are additive.

The specimens tested in this study were thermally cycled 5 times. The correlation between the model and the results suggest that only the first thermal cycle effectively hardened the matrix and produced dislocations. The local hardening of the matrix impeded further increase in dislocation density during the subsequent thermal cycles.

### **5.5 Dimensional Instability:**

From the backstress measurements made in this study on the particulate composite (figure 4.7) and unreinforced (figure 4.9) materials it is possible to estimate the maximum dimensional change which can be expected to occur in these materials. If we make the assumption that the elastic stresses in the materials in this study can be entirely transformed into plastic strain and that the backstress is a good measurement of these elastic stresses, then we can predict that the maximum dimensional instability will be given by a

strain  $\max \epsilon_{di}$

$$\max \epsilon_{di} = \sigma_B / E_m \quad (5.14)$$

where  $\sigma_B$  is the magnitude of the backstress and  $E_m$  the modulus of the matrix. For the composite material the maximum backstress measured was 200 MPa ( $T = -50^\circ\text{C}$ , offset strain of  $10^{-4}$ ) at imposed plastic strains greater than 1%. Using the modulus of 76 GPa obtained at  $-50^\circ\text{C}$  (table 4.3) gives

$$\begin{aligned} \max \epsilon_{di} &= 200 \text{ Mpa} / 76 \text{ GPa} \\ &= 2.6 \times 10^{-3} \end{aligned}$$

Repeating the calculation for the unreinforced material using a backstress of 135 MPa (figure 5.9) and the modulus of pure Al at  $-50^\circ\text{C}$  of 70 GPa (R.P. Carreker and W.R. Hibbard, 1957) gives

$$\begin{aligned} \max \epsilon_{di} &= 135 \text{ MPa} / 70 \text{ GPa} \\ &= 1.9 \times 10^{-3} \end{aligned}$$

The experimental results of the dimensional instability were obtained for plastic strain (5% to 25%) which are larger than those obtained from the Bauschinger experiments (0.2 to 2%). The magnitude of the backstress

present in the materials saturated after only 1% imposed plastic deformation (section 5.3). A comparison between the results obtained using equation 5.14 and the dimensional instability results can be done therefore assuming that the magnitude of the backstresses remains constant for imposed strains greater than those measured. When heated at 250°C the dimensional instability of the composite material is  $2.0 \times 10^{-3}$  (figure 4.14) which represents

$$2.0 \times 10^{-3} / 2.6 \times 10^{-3} \approx 77\%$$

of the maximum recoverable strain, and for the unreinforced material (figure 4.15), at the same heating temperature,

$$1.45 \times 10^{-3} / 1.9 \times 10^{-3} \approx 76\%$$

The results obtained at the heating temperature of 155°C give for both materials a dimensional change of 42% of the maximum dimensional instability according to equation 4.14.

Both materials, composite and unreinforced, therefore behave in exactly the same way in terms of their dimensional instability with respect to the magnitude of their backstress. The dimensional instability is thus clearly dependent on the backstress in the materials and the heating temperature. It is only indirectly dependent on the shape, size and volume

fraction of the second phases. The larger dimensional change in absolute terms observed in the composite material is due to the presence of a larger backstress arising from the presence of more obstacles (the SiC particles) in the microstructure which increased the capacity of the matrix to store these backstresses.

The prediction of the magnitude of the dimensional instability in a material can therefore be based on the level of backstress in the material, which itself can be based on microstructural parameters. The mechanisms involved in the relaxation processes are temperature dependent as it could be seen with the results from the two testing temperatures. The dimensional change process is therefore analogous to creep deformation where the stress imposed to the material is the internal stresses developed through plastic deformation.

The magnitude of the dimensional instability can thus be evaluated by expressing that the elastic strain in the particles transforms into plastic strain in the matrix.

$$\dot{\epsilon}_{\text{elastic}} + \dot{\epsilon}_{\text{plastic}} = 0 \quad (5.15)$$

or

$$1/E \, d\sigma/dt + \dot{\epsilon}_{\text{creep}} = 0 \quad (5.16)$$

or 
$$d\epsilon_{\text{released}}/dt = -\dot{\epsilon}_{\text{creep}} \quad (5.17)$$

The observations made throughout the experimentations on the dimensional instability showed that the change in dimension occurs mostly within an hour at the heating temperature. Very little if any change occurred between the 3<sup>rd</sup> and 24<sup>th</sup> hour of heating. This suggests that the creep is of a logarithmic type and therefore at a certain time  $t$  and temperature  $T$  we have (A.H.Cottrell, 1956)

$$\epsilon_{\text{released}} = \frac{vNkT}{A(T, \sigma)} * \log(vt) \quad (5.18)$$

where  $N$  is the number of atomic jumps,  $v, v$  and  $k$  are constants and  $A$  a constant at a given temperature and stress. The dimensional instability experiments conducted in this study concerned the maximum instability at a given temperature and therefore the rate of the dimensional change, or strain rate, was not measured during the experiments. A comparison between the creep model and the results obtained is therefore not possible but could be the subject of future work on dimensional instability that would involve the measurement of the rate of dimensional change.

## CONCLUSIONS

From the results obtained in this work regarding the tensile and Bauschinger experiments it is possible to conclude the following:

1. The rate of development through plastic deformation of the unrelaxed internal stresses in the Al-SiC<sub>p</sub> composite material can be predicted from a microscopic model (Brown and Clarke) and from a macroscopic model based on the assumption that the reinforcing phase behaves in a manner analogous to continuous longitudinal fibres.
2. The internal stresses developed in the Al-SiC<sub>p</sub> composite and unreinforced materials reach a saturation level. This level of internal stresses is attained after approximately 0.9% and 1.3% plastic strain in the case of the particulate composite and the unreinforced materials respectively.
3. The mechanism which is responsible for the saturation of the internal stresses appears to be the failure of the reinforcing phase SiC in the particulate composite material and the silicon precipitates in the unreinforced material.
4. The saturation level of internal stresses in the particulate composite and unreinforced material is dependent on the testing temperature due to the dependence of the work

hardening rate of aluminum on the testing temperature.

5. The SiC particles have a small effect on the work hardening rate of the composite at strains above 1 or 2%.

Furthermore, from the thermal cycling results we can conclude that:

6. Specimens of the particulate composite and the unreinforced materials tested in tension or in compression show an increase in their flow stress after being thermally cycled. Arsenault and Shi's model of the increase in dislocation density arising from thermal cycling is in agreement with the increase in flow stress results.

And finally from the dimensional instability results we can conclude that:

7. Both the particulate composite and the unreinforced materials have the same dimensional instability which arises due to the internal stresses developed during plastic flow. The degree of dimensional instability can be correlated with the level of internal stresses and the heating temperature.

## REFERENCES

- Allen A.J., Bourke M., Hutchings M.T., Krawitz A.D. and Windsor C.G., (1987), **Proc. of the Int. Conf. on Residual Stresses in Sc. and Tech.**, 1, p.151.
- Arsenault R.J. and Fisher R.M., (1983), **Scripta Metal.**, 17, p.67
- Arsenault R.J. and Shi N., (1986), **Mater. Sci. and Eng.**, 81, p.175
- Ashby M.F., Gelles H. and Tanner L.E., (1969), **Phil Mag.**, 19, p.757
- Atkinson J.D., Brown L.M. and Stobbs W.M., (1974), **Phil. Mag.**, 30, p.1247.
- Bate P.S. and Wilson D.V., (1986), **Acta Metall.**, 34, p.1097
- Bauschinger J., (1886), **Mittheilungen aus dem Mechanisch-Technischen Laboratorium der K. Technischen Hochschule in Munchen**, 13, p.31
- Brown L.M. and Clarke D.R., (1975), **Acta Metall.**, 23, p.821
- Brown L.M. and Stobbs W.M., (1971), **Phil. Mag.**, 23, p.1185.
- Carreker R.P.Jr. and Hibbard W.R.Jr., (1957), **Trans. AIME**, p.1157
- Carreker R.P.Jr. and Hibbard W.R.Jr., (1953), **Acta Metall.**, 1, p.654
- Chawla K.K. and Metzger M., (1972), **J. Mater. Sci.**, 7, p.34
- Cottrell A.H., (1956), **Dislocations and Plastic Flow in Crystals**, Oxford University Press.
- Derby B. and Walker J.R., (1988), **Scripta Met.**, 22, p.529
- Friedel J., (1959), **Internal Stresses and Fatigue in Metals**, Rassweiler G.M. and Grube W.L. eds., Elsevier Publishing

Co., p.220

- Garmong, G., (1974), **Metal Trans.**, 5, p.2183
- Geil G.W. and Feinberg I.J., (1969), U.S. National Bureau of Standards, Report 9997.
- Hansen N., (1977), **Acta Metall.**, 25, p.863
- Hull D. and Bacon D.J., (1984), **Introduction to Dislocations**, Pergamon.
- Hunt W.H.Jr., Brockenbrough J.R. and Magnusen P.E., (1991), **Scripta Met.Mater.**, 25, p.15
- Kelly A., (1964), **Proc.Roy.Soc.Lond.**, A282, p.63.
- Kelly A. and Lilholt H., (1969), **Phil.Mag.**, 20, p.311
- Kelly A. and MacMillan N.H., (1986), **Strong Solids**, Oxford University Press.
- Ledbetter H.M. and Austin M.W., (1987), **Mat.Sc.and Eng.**, 89, p.53
- Lilholt H., (1977), **Acta Metall.**, 25, p.587
- Lloyd D.J., (1976), **Acta Metall.**, 25, p.459
- Marschall C.W. and Maringer R.E., (1977), **Dimensional Instability**, Pergamon Press.
- Moan G.D. and Embury J.D., (1979), **Acta Metall.**, 27, p.903
- Mori T. and Narita K., (1975), **Acta Metall.**, 23, p.88
- Orowan E., (1948), **Symposium on Internal Stresses in Metals and Alloys**, The Institute of Metals, p.47
- Orowan E., (1959), **Internal Stresses and Fatigue in Metals**, Rassweiler G.M. and Grube W.L. eds., Elsevier Publishing Co., p.59
- Patterson W.G. and Taya M., (1985), **Proc. of ICCM-V**, Harrigan Jr. et al eds., TMS of AIME, p.53
- Pederson O.B., (1990), **Acta Metall. Mater.**, 38, p.1201
- Piggott M.R., (1980), **Load Bearing Fibres Composites**, Pergamon Press.
- Schmid E. and Boas W., (1950), **Plasticity of Crystals** F.A.Hughes & Co.Ltd.
- Sowerby R., Uko D.K. and Tomita Y., (1979), **Mat. Sci.& Eng.**,

41,p.43

- Sutton P.M., (1953), **Physical Review**, 91, p.816
- Tanaka K. and Mori T., (1970), **Acta Metall.**, 18, p.931.
- Taya M., (1981), **J.Comp.Mater.**, 15, p.198.
- Taya M. and Arsenault R.J. (1989), **Metal Matrix Composites Thermomechanical Behavior**, Pergamon Press.
- Taylor G.I., (1938), **J.Inst.Metals**, 62, 307
- Watt D.F., (1967), **Ph.D.Thesis**, McMaster University
- Weaver G.Q. and Olsen B.A., (1973), **Int.Conf.on SiC**, Marshall R.C., Faust J.W.Jr. and Ryan C.E. eds., University of South Carolina Press, Columbia, p.367
- Wilson D.V. and Konnan Y.A., (1964), **Acta Metall.**, 12, p.617.
- Wilson D.V., (1965), **Acta Metall.**, 13, p.807
- Wooley R.L., (1953), **Phil.Mag.**, 44, p.597
- Yoda S., Takahashi R., Wakashima K. and Umekawa S., (1979) **Metal.Trans.**, 10A, p.1796
- Yoda S., Kurihara N., Wakashima K. and Umekawa S., (1978) **Metal.Trans.**, 9A, p.1229